Published in final edited form as:

Nature. 2018 July ; 559(7713): 264–268. doi:10.1038/s41586-018-0282-0.

The purinergic receptor P2RX7 directs metabolic fitness of long-lived memory CD8+ T cells

Henrique Borges da Silva[1,2], **Lalit K. Beura**[1,3], **Haiguang Wang**[1,2], **Eric A. Hanse**[1,2], **Reshma Gore**[5], **Milcah C. Scott**[1,3], **Daniel A. Walsh**[1,2], **Katharine E. Block**[1,2], **Raissa Fonseca**[1,3], **Yan Yan**[1,2], **Keli L. Hippen**[1,4], **Bruce R. Blazar**[1,4], **David Masopust**[1,3], **Ameeta Kelekar**[1,2], **Lucy Vulchanova**[5], **Kristin A. Hogquist**[1,2], and **Stephen C. Jameson**[1,2,*]

[1]Center for Immunology, University of Minnesota, Minneapolis, MN, USA 55414

[2]Department of Laboratory Medicine and Pathology, University of Minnesota, Minneapolis, MN, USA 55414

[3]Department of Microbiology and Immunology, University of Minnesota, Minneapolis, MN, USA 55414

[4]Department of Pediatrics, University of Minnesota, Minneapolis, MN, USA 55414

[5]Department of Neuroscience, University of Minnesota, Minneapolis, MN, USA 55414

Extracellular adenosine triphosphate (eATP) is an ancient “danger signal”, used by eukaryotes to detect cellular damage[1]. In mice and humans, eATP released during inflammation and injury stimulates both innate immune activation and chronic pain through the purinergic receptor P2RX7[2–4]. It is unclear, however, whether this same pathway impacts the generation of immunological memory, a hallmark of the adaptive immune system that constitutes the basis for vaccines and protective immunity against re-infection[5,6]. We show here that P2RX7 is required for the establishment, maintenance and functionality of long-lived central and tissue-resident memory $CD8^+$ T cell populations. In contrast, P2RX7 was dispensable for generation of short-lived effector $CD8^+$ T cells. Mechanistically, P2RX7 promoted mitochondrial homeostasis and metabolic function in differentiating memory $CD8^+$ T cells, at least in part through induction of AMP-activated protein kinase (AMPK). Pharmacological inhibitors of P2RX7 provoked dysregulated metabolism and differentiation of activated mouse and human $CD8^+$ T cells *in vitro*, and transient P2RX7 blockade *in vivo* ameliorated neuropathic pain but also compromised production of $CD8^+$ memory T cells. These findings illustrate that eATP activation of P2RX7 provides a common

*Address 253 correspondence and materials/permissions requests to james024@umn.edu.

Author contributions: S.C.J. and H.B.d.S. designed, analyzed and interpreted the experiments. H.B.d.S., L.K.B., H.W., E.H., R.G., M.S., D.A.W., K.E.B., R.F. and Y.Y. performed experiments. R.G. performed spare nerve injury surgical procedures. E.H. and A.K. provided assistance with extracellular flux analysis. K.L.H., B.R.B., D.M., A.K. and K.A.H. contributed critical reagents and biological samples. S.C.J. and H.B.d.S. wrote the manuscript, with all authors contributing to editing the final text.

The authors declare no competing interests.

Data Availability Statement

The data that support the findings of this study are available from the corresponding author upon reasonable request.

currency which both alerts the nervous and immune system to tissue damage, and also promotes metabolic fitness and survival of the most durable and functionally relevant memory $CD8^+$ T cell populations.

P2RX7 is unique in the P2RX family in its activation by high eATP concentrations (such as those released by dying cells)[1,7]. P2RX7 triggering induces ion transport (including Ca^{2+} influx and K^+ efflux), but can also cause cell death by opening non-specific membrane pores[2,4,8]. Studies utilizing gene ablation and pharmacological blockade of P2RX7 suggest it supports activation and differentiation of certain effector $CD4^+$ T cell subsets, but induces death of others[7–10]. The role of P2RX7 in generating long-lived T cell memory has not been addressed. Evaluation of the response of co-adoptively transferred WT and *P2rx7*-deficient (*P2rx7*$^{-/-}$) P14 TCR transgenic $CD8^+$ T cells (P14) following acute Lymphocytic Choriomeningitis Virus (LCMV Armstrong) infection, revealed a progressive defect in maintenance of *P2rx7*$^{-/-}$ P14 in lymphoid tissues, despite normal expansion during the effector phase of the response. (Fig. 1a–c). This arose due to a profound defect in establishment of *P2rx7*$^{-/-}$ $CD62L^+$ central memory (T^{CM}), while production of effector and $CD62L^-$ effector memory (T^{EM}) was much less affected (Fig. 1b–1c). The skewing against *P2rx7*$^{-/-}$ T_{CM} may be an underestimate, since P2RX7 signaling during WT cell isolation can provoke CD62L shedding[7,8]. Further separation of memory subsets extended these findings, confirming T_{CM} were most severely compromised by P2RX7-deficiency (Extended Data Fig. 1d–e). Long-term $CD8^+$ T cell memory is mediated by T_{CM} in lymphoid tissues but by tissue-resident memory (T_{RM}) cells in non-lymphoid sites[6]. *P2rx7*$^{-/-}$ P14 showed defective T_{RM} generation, especially of the well-characterized $CD69^{hi}/CD103^{hi}$ T_{RM} population, in various non-lymphoid sites (Fig. 1d; Extended Data Fig. 1a–c). P2RX7 deficiency compromised T_{CM} and T_{RM} generation by polyclonal *P2rx7*$^{-/-}$ $CD8^+$ T cells and in response to other acute viral infections (Extended Data Fig. 1f–g), suggesting generalizable conclusions. Furthermore, *P2rx7*$^{-/-}$ P14 response to chronic LCMV infection was impaired, especially generation of CXCR5+ cells (a subset of “exhausted” CD8+ T cells that retain functionality) (Fig. 1e–f, Extended Data Fig. 1h)[11–13]. Cell surface P2RX7 expression increases following $CD8^+$ T cell activation, being highest on T_{CM} and $CD69^{hi}/CD103^{hi}$ T_{RM} (Extended Data Fig. 2a–f), corresponding with the impact of P2RX7-deficiency on these subsets. Similarly, reactivity to BzATP (an eATP analog) correlated with P2RX7 expression on memory $CD8^+$ T cell subsets, indicating P2RX7 mediates normal eATP sensitivity by memory CD8 T cells (Extended Data Fig. 2g–h). Hence the eATP sensor P2RX7 is essential for establishment of the most durable memory $CD8^+$ T cell populations in lymphoid and many non-lymphoid tissues.

We next investigated the role of P2RX7 in early differentiation of memory $CD8^+$ T cells. While *P2rx7*$^{-/-}$ P14 initially formed both short-lived (SLEC) and memory precursor (MPEC) effector cells, this was followed by a selective decline of MPEC (Fig. 2a) while SLEC maintenance was largely unaffected (Fig. 2a; Extended Data Fig. 3a). RNAseq analysis revealed minimal changes in gene expression by *P2rx7*$^{-/-}$ MPEC (Extended Data Fig. 3b), prompting evaluation of other mechanisms underlying MPEC decline. Cellular metabolism is reprogrammed during transition from activated to memory $CD8^+$ T cells[14], resulting in enhanced oxidative phosphorylation (OXPHOS), fatty acid oxidation and mitochondrial maintenance[15,16]. Previous studies suggested P2RX7 regulates metabolic

processes, although with evidence for both beneficial and detrimental effects on cell viability[7,17]. As early as 8 days post-infection, *P2rx7*$^{-/-}$ MPEC exhibited lower mitochondrial mass, mitochondrial membrane potential and glucose uptake, while SLEC were minimally affected (Fig. 2b–c, Extended Data Fig. 3c–g). Furthermore, in extracellular flux assays *P2rx7*$^{-/-}$ MPEC (but not SLEC) exhibited lower oxygen consumption rate (OCR) and reduced spare respiratory capacity – an indication of cells' metabolic resilience under stress and a trait of CD8$^+$ T_{CM}[15] (Fig. 2d–2e). These findings are consistent with reports proposing calcium influx through P2RXs promotes mitochondrial activity in short-term activated T cells[17,18]. Aerobic glycolysis was only slightly reduced in *P2rx7*$^{-/-}$ MPEC (measured by extracellular acidification rate [ECAR]; Extended Data Fig. 3h), such that the OXPHOS/aerobic glycolysis ratio (OCR/ECAR) of *P2rx7*$^{-/-}$ MPEC resembled that of SLEC (Fig. 2f). The impact of P2RX7-deficiency persisted into memory phase, *P2rx7*$^{-/-}$ P14 displaying defective glucose uptake, mitochondrial maintenance and function, and fatty acid uptake – most of these defects more substantially affected T_{CM} over T_{EM} (Fig. 2g–2i; Extended Data Fig. 3i–m). Thus, our findings suggested the eATP receptor P2RX7 is critical for mitochondrial homeostasis and normal metabolic function in differentiating memory CD8$^+$ T cells.

Metabolic defects might be predicted to compromise T cell survival. Indeed, basal proliferation of P2RX7-deficient memory P14 was normal, but they exhibited increased cell death (Extended Data Fig. 4a–c). Correspondingly, *P2rx7*$^{-/-}$ MPEC and T_{CM} exhibited slightly reduced protein expression of the anti-apoptotic factor Bcl2 and transcription factors Tcf1 and Eomes (associated with T_{CM} differentiation[19]), while SLEC and T_{EM} populations were much less affected (Extended Data Fig. 4d–4f). Similar outcomes resulted when WT and *P2rx7*$^{-/-}$ P14 cells were adoptively transferred separately (data not shown). Survival of T_{CM} is supported by IL-7 and IL-15[5], but although *P2rx7*$^{-/-}$ P14 displayed reduced cell surface IL-7Rα expression, they showed normal dependence on IL-15 for homeostasis (Extended Data Fig. 4g–i). Furthermore, *P2rx7*$^{-/-}$ P14 cells outcompeted WT cells for lymphopenia-induced proliferation (Extended Data Fig. 4j–k) –a homeostatic response to IL-7 and IL-15 that does not involve strong TCR stimulation[20]. Together, these data argue against impaired cytokine sensitivity as a basis for defective *P2rx7*$^{-/-}$ CD8$^+$ T_{CM} maintenance.

To explore how P2RX7 selectively controlled metabolism of differentiating CD8$^+$ memory T cells, we utilized *in vitro* assays in which activated CD8$^+$ T cells cultured with IL-2 or IL-15 acquire effector- or memory-like properties, respectively[15,21]. WT and *P2rx7*$^{-/-}$ P14 responded similarly to IL-2, but in IL-15 cultures *P2rx7*$^{-/-}$ cells progressively declined in viability (Fig. 3a), analogous to defective memory survival *in vivo* (Extended Data Fig. 4c). Furthermore, 72h after IL-15 culture, *P2rx7*$^{-/-}$ P14 developed profound decreases in maximum OCR levels and SRC (Fig. 3b–3c), within the viable population (Extended Data Fig. 5a). IL-15-polarized *P2rx7*$^{-/-}$ P14 also displayed defective aerobic glycolysis (Extended Data Fig. 5b) and decreased mitochondrial mass and membrane potential (Extended Data Fig. 5c–5d). These results are unlikely to reflect altered cytokine sensitivity, since *P2rx7*$^{-/-}$ and WT P14 showed similar pSTAT5 induction and re-expression of CD62L in IL-15 cultures (Extended Data Fig. 5e–5f)[21] and normal expansion (Extended Data Fig. 5g). IL-2 polarized *P2rx7*$^{-/-}$ P14 showed some dysfunction (reduced mitochondrial mass; impaired

aerobic glycolysis), suggesting P2RX7 also impacts effector metabolism, although *P2rx7*$^{-/-}$ effector cell generation was normal *in vivo* (Fig. 2a). Hence, our data demonstrated P2RX7's ability to control metabolism in nascent memory CD8^{+} T cells could be modelled *in vitro*.

Metabolic programming in T cells entails mitochondrial remodeling and memory CD8^{+} T cells develop fused mitochondria correlating with more efficient OXPHOS[22]. Analysis of mitochondrial ultrastructure showed IL-15-polarized *P2rx7*$^{-/-}$ P14 fail to form fused mitochondrial networks seen in WT cells, more closely resembling IL-2-cultured effector cells (Fig. 3d; Extended Data Fig. 6a). Furthermore, *in vitro*- and *in vivo*-activated *P2rx7*$^{-/-}$ P14 exhibited increased proton leak during respiration at multiple stages of differentiation (Extended Data Fig. 6b–d), suggesting mitochondrial damage[22]. These data indicated P2RX7 deficiency impairs the dynamic mitochondrial reorganization associated with memory CD8^{+} T cell differentiation. Opa1 drives mitochondrial fusion in T cells[22], and Opa1 expression was reduced in IL-15-polarized *P2rx7*$^{-/-}$ P14 (Extended Data Fig. 6e–f). However, Opa1 levels were proportional to total mitochondrial protein (Extended Data Fig. 6g–h) and it is unclear whether reduced Opa1 expression is a cause or consequence of dysregulated mitochondrial homeostasis in *P2rx7*$^{-/-}$ CD8+ T cells.

It was possible that P2RX7 deficiency impacted T cells prior to activation and differentiation. However, metabolism of naïve *P2rx7*$^{-/-}$ CD8^{+} T cells was normal (Extended Data Fig. 7a–7c). Furthermore, treatment with A-438079 (a highly-specific P2RX7 inhibitor[23]) during CD8^{+} T cell activation and IL-15-polarization resulted in dysregulated metabolism similar to P2rx7$^{-/-}$ CD8^{+} T cells (Fig. 3e). These findings also provided an opportunity to extend our observations to human T cells. Treatment with A-438079 caused significant loss of OXPHOS and aerobic glycolysis in activated human T cells (Fig. 3f; Extended Data Fig. 7d), and substantial decrease in their proliferation and cytokine production (Fig. 3g–3h), yet short-term survival was not impacted (Extended Data Fig. 7e). Hence, while having some species-specific effects, blockade of P2RX7 compromises metabolism of both human and mouse activated CD8^{+} T cells.

Our data suggested eATP would promote CD8^{+} T cell metabolism and growth. Indeed, eATP blockade (using the ATP-diphosphatase Apyrase, or the competitive inhibitor oATP) impaired expansion and OCR of IL-15 cultured P14 CD8^{+} T cells, while low concentrations of BzATP had the opposite effect (Fig. 3i; Extended Data Fig. 8a–e). Such doses of BzATP induced calcium mobilization but minimal pore formation (Extended Data Fig. 8f), consistent with studies suggesting P2RX7-induced calcium flux enhances mitochondrial function[7,10,17]. None of these compounds are P2RX7 specific, yet their effects on CD8^{+} T cells were entirely P2RX7-dependent (Fig. 3i; Extended Data Fig. 8a–f). Furthermore, short-term P2RX7 inhibition blocked OCR in IL-15 cultured CD8^{+} T cells (Extended Data Fig. 8g). Hence, these studies suggest physiological levels of eATP promote mitochondrial metabolism and growth of activated CD8^{+} T cells, in a pathway requiring P2RX7.

An important issue was the source of eATP triggering P2RX7 signaling. While eATP is released from tissues during infection and injury[1,7], eATP is also exported by healthy activated T cells through Pannexin 1 (PANX1) channels, which are themselves triggered by P2RX7 signaling[24]. In this way, activated T cells could autonomously maintain P2RX7

signaling by both exporting and responding to eATP, perpetuating mitochondrial function through sustained calcium ion influx (and/or other functions of P2RX7). Both extrinsic and PANX1 derived eATP have been proposed to impact effector $CD4^+$ T cell differentiation[10]. Interestingly, inclusion of the PANX1 inhibitor Probenecid during *in vitro* $CD8^+$ T cell memory-like cell generation caused impaired OXPHOS and reduced SRC similar to *P2rx7*$^{-/-}$ $CD8^+$ T cells (Fig. 3j–3k), suggesting PANX1 can regulate the same metabolic pathways. Consistent with a role for P2RX7/PANX1 in ATP export, intracellular ATP concentrations were elevated while extracellular ATP concentrations were decreased in *P2rx7*$^{-/-}$ effector $CD8^+$ T cells, PANX1 being critical for eATP (Extended Data Fig. 8h,i).

Elevated intracellular ATP concentrations could lead to impaired activation of AMPK, which controls adaptation to environmental stress[25], restrains mTOR activity and promotes transition from effector to memory $CD8^+$ T cells[14,26]. Indeed, mTOR activity (indicated by pS6 levels) was elevated in memory *P2rx7*$^{-/-}$ T cells (Extended Data Fig. 8j). More directly, IL-15-polarized *P2rx7*$^{-/-}$ $CD8^+$ T cells exhibited decreased phosphorylation of the AMPK target Acetyl-CoA carboxylase (pACC; Fig. 3l). AMPK is also activated by intracellular calcium[14], and stimulation with BzATP at doses promoting efficient calcium flux (Extended Data Fig. 8f) increased the pACC/pS6 ratio in WT but not *P2rx7*$^{-/-}$ $CD8^+$ T cells (Extended Data Fig. 8k). Furthermore, *in vitro* treatment with AICAR (a pharmacological AMPK activator) largely corrected defective OCR and survival in *P2rx7*$^{-/-}$ CD8+ T cells (Fig. 3m; Extended Data Fig. 8l). *In vivo*, activation of AMPK using metformin enhanced generation of *P2rx7*$^{-/-}$ $CD8^+$ T_{CM} and T_{RM} (while minimally impacting circulating T_{EM}), and partially or completely restored normal mitochondrial mass and membrane potential in *P2rx7*$^{-/-}$ P14 T_{CM} (Fig. 3n; Extended Data Fig. 8m–o). Similarly, transient mTOR blockade with rapamycin improved production of *P2rx7*$^{-/-}$ T_{CM} (Fig. 3o; Extended data 8p). Collectively, these data indicate P2RX7 activates AMPK which, perhaps via mTOR inhibition, supports generation of long-lived memory CD8+ T cells.

In vitro cytotoxicity and Granzyme B expression was normal in *P2rx7*$^{-/-}$ P14 effector cells (data not shown), but the functionality of *P2rx7*$^{-/-}$ memory $CD8^+$ T cells was unclear. Equivalent numbers of WT or *P2rx7*$^{-/-}$ memory P14 were independently evaluated for response to vaccinia virus expressing gp33 (Fig. 4a), revealing reduced recall expansion (Fig. 4b) and viral control (Fig. 4c) by *P2rx7*$^{-/-}$ P14 cells. Impaired LCMV clone 13 viral control was also observed in polyclonal *P2rx7*$^{-/-}$ mice (Extended Data Fig. 9a). *P2rx7*$^{-/-}$ P14 recall responses to recombinant *Listeria* were also blunted, correlating with increased cell death rather than impaired proliferation (Extended Data Fig. 9b–9f). Likewise, following local antigen challenge of female reproductive tract T_{RM} (using transcervical peptide stimulation$_{27}$), significantly fewer *P2rx7*$^{-/-}$ P14 T_{RM} produced IFN-γ or Granzyme B, accompanied by reduced "bystander" $CD8^+$ T cell activation and local dendritic cell maturation (Fig. 4d, Extended Data Fig. 9g,h). These data demonstrate P2RX7 is critical not only for memory $CD8^+$ T cell maintenance but also their function.

P2RX7 is considered a promising pharmacological target for chronic pain treatment[7,28]. Thus, we investigated whether P2RX7 blockade therapies designed to treat neuropathic pain would impede generation of $CD8^+$ T cell memory, developing a combined model of spared nerve injury with LCMV infection (Extended Data Fig. 9i–k). Transient *in vivo* treatment

with A-438079 significantly attenuated nerve injury-induced hypersensitivity (Fig. 4e) and, in parallel, significantly decreased production of memory $CD8^+$ T cells, especially T_{CM}, 1 month later (Fig. 4f). Furthermore, A-438079 treatment during the week following LCMV infection reduced subsequent generation of memory and MPEC (but not SLEC) P14, resembling the defects of *P2rx7*$^{-/-}$ CD8+ T cells (Extended Data Fig. 9l–n). A-438079 also impaired $CD8^+$ T_{CM} and T_{RM} generation in LCMV infected BALB/c mice, which express a functionally distinct *P2rx7* allele[7] (Extended Data Fig. 9o). Interestingly, P2RX7-blockade caused loss of pre-existing memory $CD8^+$ T cells, especially T_{CM}, suggesting P2RX7 is required for maintenance of $CD8^+$ T cell memory (Fig. 4g, Extended Data Fig. 9p). Hence, therapeutic P2RX7-inhibition may inadvertently compromise development or maintenance of long-lived $CD8^+$ T cell memory.

A paradigm shift in immunology came with understanding that detection of pathogen- and danger-associated molecular patterns are critical to spark immune reactivity[29,30]. eATP is one of these triggers, representing a primordial mechanism for indicating tissue injury and inflammation[1], however, the impact of this pathway on adaptive immune memory was unclear. We show here that the eATP sensor P2RX7 plays a hitherto unsuspected intrinsic role in supporting generation of long-lived memory $CD8^+$ T cells through driving their metabolic reprogramming and mitochondrial maintenance. Thus, eATP, produced by damaged tissue or exported by activated cells, not only triggers innate immune activation and inflammatory nociception but plays an additional critical role by promoting durable adaptive immunological memory (Extended Data Fig. 10).

Online methods

Mice and infections

Six- to 8-week old C57BL/6 (B6) and B6.SJL (expressing the CD45.1 allele) mice were purchased from Charles River (via the National Cancer Institute). *P2rx7*$^{-/-}$, *Rag2*$^{-/-}$ and CX3CR1$^{gfp/gfp}$ mice were obtained from Jackson Laboratories. LCMV-D^bGP33-specific TCR transgenic P14 mice were fully backcrossed to B6 and *P2rx7*$^{-/-}$ mice, with introduction of CD45.1 and CD45.2 congenic markers for identification. Mice were infected with either LCMV Armstrong strain (2×10^5 PFU, intraperitoneally (i.p.)), LCMV Clone 13 strain (2×10^6 PFU, intravenously (i.v.)) or with VSV-OVA (1×10^6 PFU, i.v.). In some experiments, the LCMV viral titers in the kidneys of Clone 13-infected mice were evaluated by standard plaque assay. In challenge experiments, mice were first infected with LCMV and, 6–8 weeks later, inoculated with *Listeria monocytogenes* (Lm)-GP33 (8×10^4 CFU). For vaccinia challenge experiments, memory P14 WT and *P2rx7*$^{-/-}$ cells were sort purified from CD45.1 congenic mice that had received WT or *P2rx7*$^{-/-}$ P14 cells, respectively, and were infected with LCMV 4 weeks before sacrifice. Memory WT or *P2rx7*$^{-/-}$ P14 cells (2×10^4) were separately transferred into naïve CD45.1 congenic recipient mice, which were then infected with vaccinia virus encoding the LCMV epitope gp33 (VacV-gp33). After 7 days, mice were sacrificed, spleens were harvested to examine cell expansion, and ovaries were isolated for viral titer assessment by plaque assay. Viral titration was performed following a previously described protocol[31]. Briefly, ovaries were homogenized in RPMI +1% FBS containing Penicillin and Streptomycin with the aid of a handheld homogenizer

and serial dilutions of homogenates were plated on 143B cells (ATCC® CRL-8304™) for viral growth. After two days, plaques were enumerated after crystal violet staining. Transcervical challenges with GP33 peptide (50 μg/mouse) were performed as described before[32]. Animals were maintained under specific-pathogen-free conditions at the University of Minnesota. All experimental procedures were approved by the institutional animal care and use committee at the University of Minnesota.

Administration of A-438079 in mice

A-438079 (Sigma-Aldrich) (in 0.5% DMSO in PBS) was administered to mice i.p. daily during the indicated treatment periods at a daily dose of 80 mg kg^{-1} (which was previously shown to inhibit nociceptive pain in murine models[33]). Three different regimens of administration were used, in which A-438079 was given between days 1 and 7, between days 4 and 6 or between days 40 and 50 relative to LCMV infection. Control mice received daily vehicle injections (0.5% DMSO in PBS) during the same time periods.

Administration of metformin and rapamycin in mice

Metformin (Sigma-Aldrich) was administered to mice i.p. daily between days 1 and 7 after LCMV infection. The daily dose of metformin was 200 mg kg^{-1}, which was previously shown to potentiate memory $CD8^+$ T cell generation[34]. Control mice received daily vehicle injections (0.1% DMSO in PBS) during the same period. Rapamycin (LC Laboratories) was administered to mice i.p. daily between days 4 and 8 after LCMV infection. The dose of rapamycin was 75 μg kg^{-1}/d, as previously used during acute viral infection[35]. Control mice received daily vehicle injections (0.01% DMSO in PBS) during the same period.

Flow cytometry

Lymphocytes were isolated from tissues including spleen, inguinal lymph nodes, cervical lymph nodes, blood, lung, gut intestinal epithelium, gut intestinal lamina propria, female reproductive tract, kidney and salivary glands as previously described[36,37]. During isolation of lymphocytes from non-lymphoid tissues, 50μg of Treg-Protector (anti-ARTC2.2) nanobodies (BioLegend) were injected i.v. 15–30 minutes prior to mouse sacrifice. Direct *ex vivo* staining and intracellular cytokine staining were performed as described previously[37,38] with fluorochrome-conjugated antibodies (purchased from BD Biosciences, BioLegend, eBioscience, Cell Signaling Technology, Tonbo or Thermo Fisher Scientific). CXCR5 staining was performed as previously reported[39]. To detect LCMV-specific $CD8^+$ T cell responses, tetramers were prepared as described previously[40]. For discrimination of vascular-associated lymphocytes in non-lymphoid organs, *in vivo* i.v. injection of PE-conjugated CD8α antibody was performed as described[41]. Among LCMV-specific $CD8^+$ T cells, the following markers were used to distinguish these respective populations: T_{CM} ($CD44^+CD62L^+$), T_{EM} ($CD44^+CD62L^-$ $CD127^+$), T_{RM} (i.v.$CD8\alpha^-CD69^{+/-}CD103^{hi/int/lo}$) LLECs ($CD44^+CD62L^-KLRG1^+CX3CR1^{hi}$), MPECs ($CD127^+KLRG1^-$), SLECs ($CD127^-KLRG1^+$). For detection of *in vivo* proliferation, cells were stained with Ki-67 using the Foxp3 kit for fixation and permeabilization. Alternatively, proliferation was assessed by BrdU incorporation as described before[42]. For survival assessment, cells were stained with Live/Dead (Tonbo Biosciences) and, when mentioned, with Annexin V-FITC (eBiosciences). For assessment of homeostatic proliferation, WT or *P2rx7*$^{-/-}$ P14 cells were

stained with CFSE and transferred into Rag2−/− mice (2×10^6 cells per mice) as previously[43]. The numbers and percentages of $CFSE^{low}$ cells were assessed within the next 3 weeks. After this period, mice were sacrificed and the proliferation of spleen P14 cells was assessed. For measurement of mitochondrial mass and membrane potential, cells were incubated with MTG (Thermo Fisher Scientific) and TMRE (Cell Signaling Technology) simultaneously for 15 min at 37°C prior to *ex vivo* staining. For assessment of glucose uptake, cells were incubated with 50 μg/ml of 2-NBDG (Cayman Chemicals) for 2 h at 37°C prior to *ex vivo* staining. For measurement of intracellular fatty acid levels, cells were incubated with 1 μg/ml of $Bodipy^{493/503}$ (Thermo Fisher Scientific) for 20 min at 37°C prior to *ex vivo* staining. For assessment of proliferation upon *in vitro* stimulation, $CD8^+$ T cells were labeled with Cell Tracer Violet (CTV; Life Technologies) and after stimulation were *ex vivo* stained. For detection of intracellular factors such as Bcl-2, Eomes and TCF1, surface-stained cells were permeabilized, fixed and stained by using the eBioscience Foxp3 staining kit, according to manufacturer instructions. For intracellular detection of pS6, *ex vivo* stained cells were fixed, permeabilized using the Phosflow Perm Buffer III (BD Biosciences) and stained with pS6 for 1 h at room temperature. For intracellular detection of pACC, cultured cells were fixed with Paraformaldehyde 1%, permeabilized with 90% Methanol and stained with pACC for 20 min at room temperature. Surface staining was performed after fixation to minimize effects on AMPK signaling. For assessment of Calcium influx, cells were stained with surface markers, then incubated for 1h at 37°C with 1 μM Indo-1 (Thermo Fisher Scientific) then washed, while for detection of large molecular weight pore formation, DAPI (Thermo Fisher Scientific; 1 μM) as added to the cell culture just before assay. In both cases, cells were analyzed by kinetic flow cytometry, a baseline reading being determined for 1 minute then Bz-ATP (Sigma-Aldrich; 100 or 300 μM) added and the analysis continued for the remaining ~30 min. The ratios between Bound Indo-1 and Free Indo-1 were used as a measurement for Calcium influx and uptake of DAPI was measured in the BV-421 channel. Flow cytometric analysis was performed on a LSR II or LSR Fortessa (BD Biosciences) and data was analyzed using FlowJo software (Treestar).

Cell sorting

Cell sorting was performed on a FACS Aria III device (BD Biosciences). RNA-Seq and Extracellular flux analysis experiments were performed on $KLRG1^+CD127^-$ (SLEC) and $KLRG1^-CD127^+$ (MPEC) $CD8^+$ T cells sorted from mice 8 or 14 days post-LCMV infection, respectively. The population purity after cell sorting was >95% in all experiments.

RNA-seq analysis

8-day post-LCMV infection MPECs and SLECs were first homogenized using QIAshredder columns (Qiagen) and RNA was then extracted using an RNeasy kit (Qiagen) following manufacturer instructions. Following quality control, total RNA samples were processed with the Illumina TotalPrep-96 RNA Amplification Kit for HighThroughput RNA Amplification for Array Analysis, and read in a HiSeq 2500 System (High Output sequencing, Paired End Read, 125 bp).

Metabolic assays

OCR and ECAR were assessed using a 96-well XF Extracellular flux analyzer, according to the manufacturer instructions (Seahorse Bioscience). Spare respiratory capacity (SRC), OCR/ECAR ratios and proton leak were defined as described previously[44,45]. In some extracellular flux assays, Bz-ATP (300 μM), oATP (EMD Millipore; 50 μM) or Apyrase (New England Biolabs; 10 U/ml) were added either at the port or 1h prior to analysis. In other experiments, A-438079 (25 μM) was added 6h prior analysis. Intracellular ATP concentrations were measured by using the ATP determination kit (Life Technologies). To assess the levels of extracellular ATP, WT or *P2rx7*$^{-/-}$ P14 cells were *in vitro* activated and polarized with IL-2 or IL-15 as described above, except the cytokine polarization cultures were performed in Transwells (Corning Inc.). After 24h of polarization, the transwells were transferred to new wells and the plates were centrifuged at 50 RPM for 1 min. The supernatant below the transwells was quantified for ATP concentration as described above. In all transwells, a combination of the plasma membrane ATPase inhibitor Ebselen (30μM; Cayman Chemical) and the ecto-ATPase inhibitor ARL 67156 trisodium salt hydrate (100μM; Sigma-Aldrich) was added 1h prior to evaluation, to inhibit ATPase activity[46]. In some samples, a Pannexin 1 inhibitor (^{10}Panx, Tocris) was added 20h prior to assessment.

Transmission electron microscopy

Cells were fixed in 2.5% Glutaraldehyde in 100 mM sodium cacodylate, followed by post-fixation in 1% Osmium tetroxide. After extensive washing, samples were stained in 1% Uranyl Acetate for 30 minutes in the dark, then washed again. Samples were dehydrated in Ethanol and embedded in Eponate Resin. Cells were imaged using a JEOL 1200 EXII transmission electron microscope equipped with a SIS MegaView III high resolution CCD camera (1376 × 1032-pixel format, 12 bit). Mitochondrial areas were calculated using the ImageJ software (NIH).

Protein quantification experiments

Western blotting of total protein lysates was performed as described before[44]. The following antibodies were used: Opa1 (BD Biosciences) and beta-Actin (Cell Signaling Technologies). Primary incubations were followed by incubation with secondary HRP-conjugated antibodies (Santa Cruz Biotechnology). Blots were revealed using the Biomax MR film (Kodak).

To quantify the total mitochondrial protein amounts, mitochondria were isolated from experimental P14 cells by using the Qproteome Mitochondria Isolation Kit (QIAgen), following the manufacturer instructions. The mitochondria protein extracts were quantified using the Pierce BCA protein kit (Thermo Fisher).

In vitro culture experiments

P14 splenocytes from naïve mice were stimulated for 72 h with gp33 peptide (1 μM, KAVYNFATM, New England Peptide) and IL-2 (10 ng/ml). When indicated, Probenecid (100 μM, Sigma-Aldrich) or A-438079 (25 μM) was added to the cultures (48 h prior to analysis). Where indicated, P14 cells were isolated with mouse CD8^{+} T cell isolation kit (Miltenyi Biotech) 72h after initial activation, and incubated for an additional 72 h or 7 days

with IL-2 or IL-15 to induce generation of effector-like and memory-like populations, as described previously[47]. Cell numbers were assessed by Neubauer chamber counting. Survival was analyzed by Trypan blue staining during microscope counting, and confirmed by Live-Dead (Tonbo Biosciences) staining using flow cytometry. For all experiments, complete RPMI media (RPMI 1640 supplemented with 10% FBS, 100 U/ml penicillin/streptomycin, 2 mM L-glutamine) was used. In some experiments, IL-2 or IL-15-cultured P14 cells were cultured in the presence of 100μM – 1mM BzATP for 72 h and cell numbers and survival were measured as indicated. In other experiments, IL-2 or IL-15-cultured P14 cells were cultured in the presence of either 50 – 100μM oATP or with 10 U/ml Apyrase for 72 h, and cell numbers and survival were measured as indicated. In some experiments, IL-2 or IL-15-cultured P14 cells were cultured in the presence of 500μM of AICAR (Sigma-Aldrich) for 72 h and cell numbers and survival were measured as indicated. For extracellular flux analysis, AICAR was added 6 h prior to assay. Survival of WT and *P2rx7*$^{-/-}$ cells in extracellular flux assay medium was assessed by the WST-1 viability assay according to manufacturer instructions (Sigma-Aldrich).

Human CD8^{+} T cell studies

Resting CD8^{+} T cells were isolated from Ficoll-purified PBMC isolated from leukapheresis products (Memorial Blood Center, St. Paul, MN) in a two-step process by first depleting CD25^{+} cells using using (cGMP)-grade anti-CD25 microbeads (Miltenyi Biotec, Auburn, CA) on an AutoMACS (Miltenyi Biotec). CD8+ cells were then purified from the CD25^{-} fraction using negative selection (CD8^{+} T cell isolation kit, Miltenyi Biotec). Purified cells were stimulated for 72 h with αCD3/αCD28 beads (InVitrogen) + IL-2 (300U/ml). After 20 h, A-438079 (25μM) or PBS was added to the cultures. Cell numbers were analyzed by Neubauer chamber counting. Survival was analyzed by Trypan blue staining during microscope counting and confirmed by Live-Dead (Tonbo Biosciences) staining using flow cytometry.

Spared nerve injury (SNI) model and measurement of mechanical sensitivity

The SNI model produces substantial and prolonged changes in mechanical sensitivity and cold responsiveness that closely mimic the cutaneous hypersensitivity associated with clinical neuropathic pain[48]. SNI surgeries were performed under isoflurane anesthesia as described[49]. Fourteen days after SNI the mice were infected with LCMV and treated with A-438079 (80 mg kg-1) or vehicle on days 1–7 post-infection. For assessment of mechanical sensitivity, mechanical withdrawal thresholds were tested using von Frey filaments. Mice were acclimated for at least 30 min in the testing environment within a plastic box on a raised metal mesh platform. A logarithmically increasing set of 8 von Frey filaments (Stoelting, Illinois), labeled from 0.07 to 6.0 g were utilized. These were applied perpendicular to the ventral-lateral hindpaw surface with sufficient force to cause a slight bending of the filament. A rapid withdrawal of the paw away from the stimulus fiber within 4s was deemed as a positive response. Using an up-down statistical method[50], the 50% withdrawal threshold was calculated for each mouse and then averaged within the experimental groups. Mechanical withdrawal thresholds were measured at baseline, on day 14 post-SNI, and 6h after the last drug treatment.

Statistical analysis

Data were subjected to the Kolmogorov-Smirnov test to assess Gaussian distribution. Statistical differences were calculated by using unpaired two-tailed Student's t-test or One-way ANOVA with Tukey post-test where indicated. All experiments were analyzed using Prism 5 (GraphPad Software). P values of <0.05 (*), <0.01 (**) or <0.001 (***) indicated significant differences between groups. A table with exact p-values for all experiments is provided in Supplementary Table 1.

Extended Data

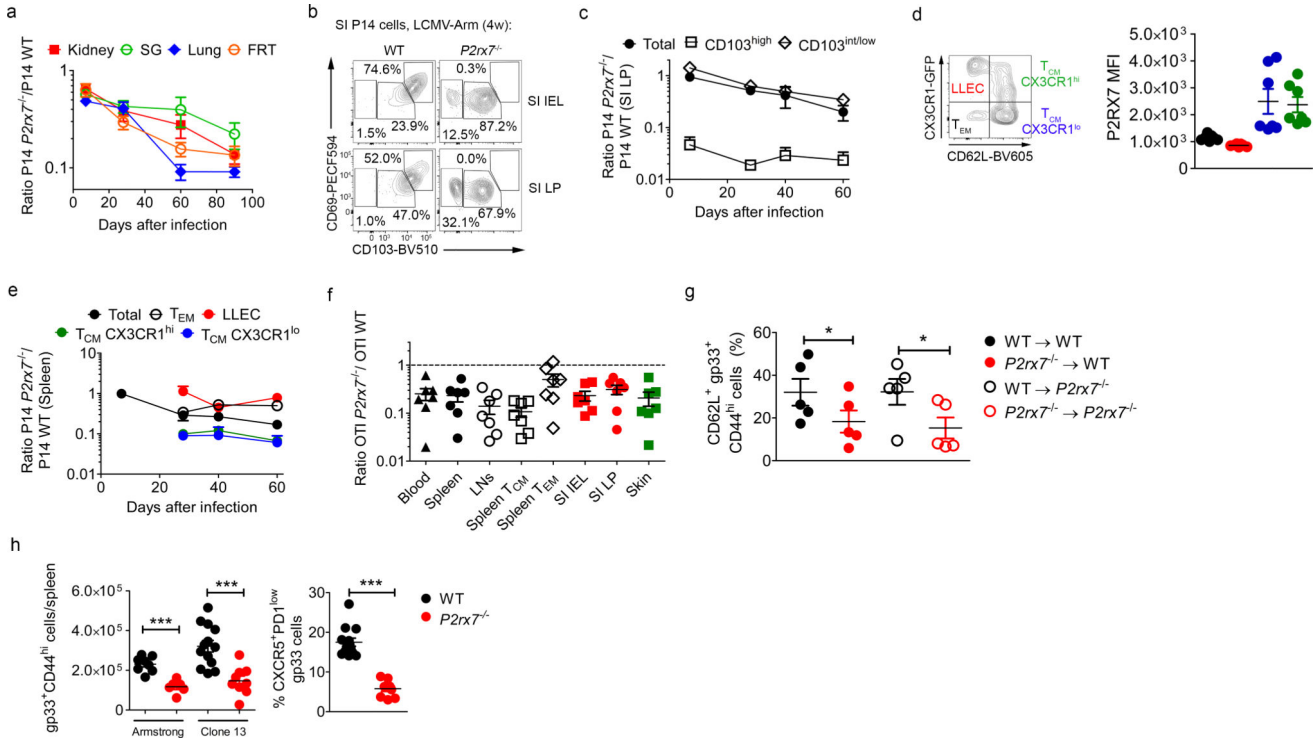

Ext. Data Fig. 1. P2RX7 is required for CD103^{hi} T_{RM} and T_{CM} generation upon acute viral infection, and for establishment of Ag-specific CD8$^+$ T cells upon chronic viral infection

(a–e), WT and *P2rx7*$^{-/-}$ P14 CD8$^+$ T cells were mixed 1:1, co-adoptively transferred into B6.SJL mice that were subsequently infected with LCMV, and donor cells identified as in Fig. 1. (data from 3–4 independent experiments, n=4 FRT and n=5–7 other organs from all experiments). **(a)**, *P2rx7*$^{-/-}$/WT P14 ratios in different non-lymphoid organs over time. **(b)**, Flow cytometric plots showing CD69 and CD103 co-expression by WT and *P2rx7*$^{-/-}$ P14 cells from SI IEL and SI LP 4-weeks post-infection (representative of 3 experiments). **(c)**, *P2rx7*$^{-/-}$/WT P14 ratios for CD103^{hi}, CD103^{int} and CD103^{low} subsets among SI LP over time. **(d–e)**, We also evaluated the role of P2RX7 in the generation and maintenance of memory CD8$^+$ T cell subsets based on CX3CR1 expression. **(d)** representative plot depicting the subpopulations studied (left) and P2RX7 median in these subsets (right). **(e)** Ratio of *P2rx7*$^{-/-}$ to WT P14 CD8$^+$ T cells in spleen, gated on indicated subsets. Data from 2–3 independent experiments, n=4–7 mice total. **(f)** WT and *P2rx7*$^{-/-}$ OT-I CD8$^+$ T cells were mixed 1:1 and co-adoptively transferred into B6 mice subsequently infected with VSV-OVA

(two independent experiments, n=7 from all experiments). WT to *P2rx7*$^{-/-}$ OT-I ratio in indicated tissues was determined 4-weeks post VSV-OVA infection. **(g)**, The indicated radiation bone marrow chimeras were generated and infected with LCMV. Percentages of splenic D^{b}/gp33-tetramer binding ("gp33^{+}") CD8^{+} T$_{CM}$ was determined 8-weeks post-infection with LCMV (data from two independent experiments, n=5 from all experiments). **(h)** WT or *P2rx7*$^{-/-}$ mice were infected with LCMV-Arm or LCMV-Cl13, and the numbers (left) and percentages of CXCR5^{+}PD1^{low} (right) gp33^{+} CD8^{+} T cells were evaluated 4 weeks after infection (n=6–13 from all experiments). **(a,c–h)** mean ± SEM is shown; **(g–h),** Two-tailed Student's t-test, *P≤0.05, **P≤0.01, ***P≤0.001.

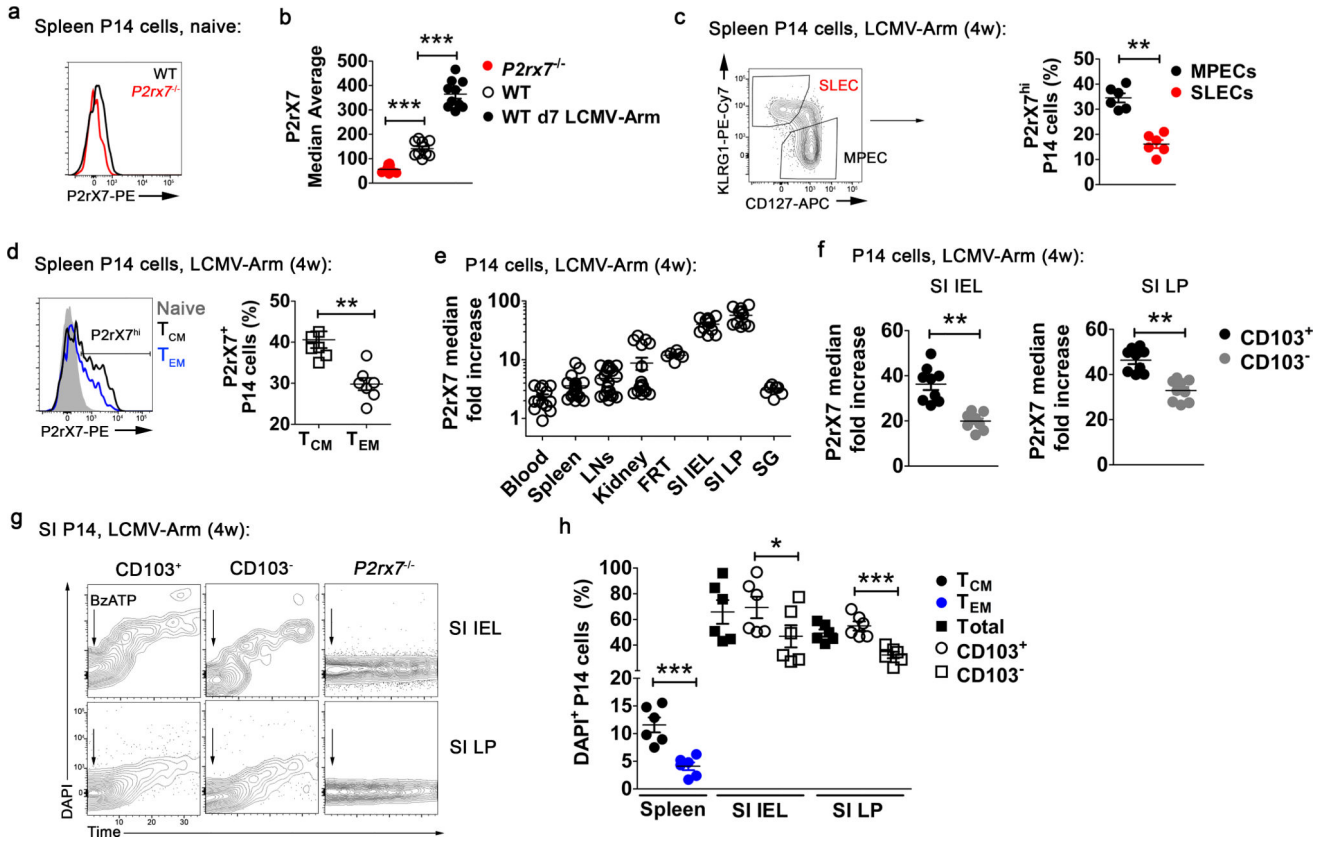

Ext. Data Fig. 2. Long-lived memory CD8^{+} T cells express higher levels of functional P2RX7

(a), Flow cytometry histograms for P2RX7 staining on naïve WT or *P2rx7*$^{-/-}$ P14 cells (representative of 3 experiments). (**b**), Median average values for P2RX7 staining on naïve WT and *P2rx7*$^{-/-}$, and WT P14 cells 7d post-LCMV infection (data from three independent experiments, n=10 total). **(c–h)**, Indicated subsets of adoptively transferred WT P14 CD8^{+} T cells from listed tissues were assayed for P2RX7 expression and functional response to the P2RX7 agonist BzATP following priming with LCMV for indicated time (data from three independent experiments, n=6–21 from all experiments). **(c,d)**, Percentage of P2RX7^{hi} WT P14 cells in MPEC and SLEC **(c)** and T$_{CM}$ and T$_{EM}$ subsets **(d)** at 4-weeks post-infection. **(e)**, P2RX7 median fold increase (relative to expression in naïve CD8^{+} T cells, showed as a dashed line) of P14 cells in blood, lymphoid and non-lymphoid organs (4-weeks post-infection). **(f)**, P2RX7 median fold increase (relative to naïve CD8+ T cells) of CD103^{+} vs

CD103$^-$ P14 cells in SI IEL and SI LP. **(g–h)**, adoptively transferred and LCMV primed WT and *P2rx7*$^{-/-}$ P14 cells were incubated with DAPI then stimulated during flow cytometry with 300 μM Bz-ATP (which mediates P2RX7 pore opening and DAPI uptake). **(g)** shows flow cytometry plots of DAPI uptake by SI IEL and SI LP WT and *P2rx7*$^{-/-}$ P14 CD8$^+$ T cells over 30 minutes time (representative of 6 samples), while **(h)** shows compiled data for percentage DAPI$^+$ P14 cells (defined as the percentage above *P2rx7*$^{-/-}$ DAPI levels 5 minutes after Bz-ATP stimulation) in spleen, SI IEL and SI LP P14 cells (n=6 from all experiments). **(b–f, h)** mean ± SEM is shown; **(b)**, One-way ANOVA with Tukey post-test; **(c,d,f,h)**, Two-tailed Student's t-test; *P≤0.05, **P≤0.01, ***P≤0.001.

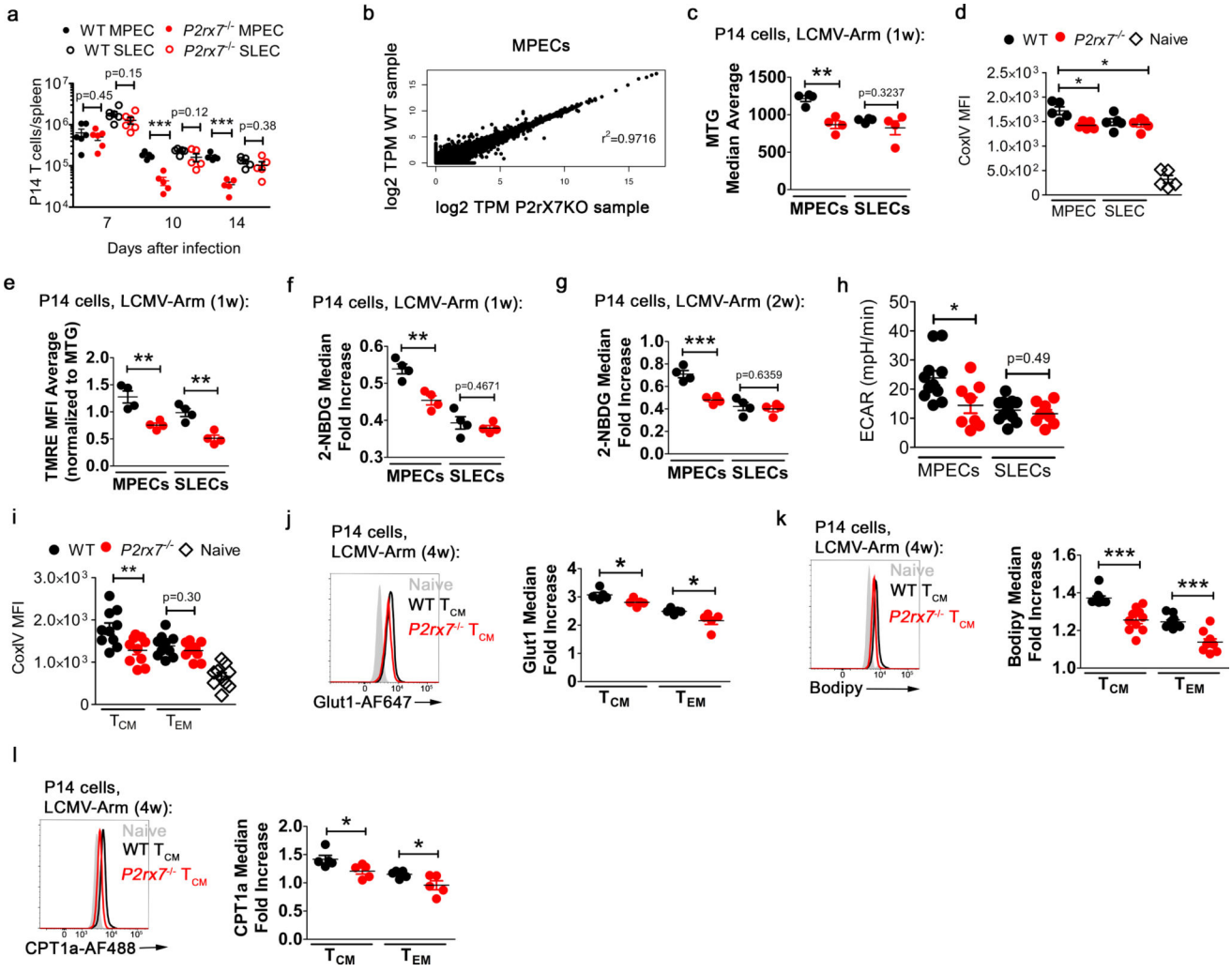

Ext. Data Fig. 3. P2RX7 is required for optimal metabolism of MPECs and T_{CM} cells

WT (black) and *P2rx7*$^{-/-}$ (red) P14 CD8$^+$ T cells were mixed 1:1, co-adoptively transferred into B6.SJL mice that were subsequently infected with LCMV, and donor cells identified as in Fig. 1. **(a)** Numbers of WT and *P2rx7*$^{-/-}$ P14 MPECs and SLECs in spleens (Three independent experiments, n=5–6 from all experiments). **(b)** Gene expression profile from WT versus *P2rx7*$^{-/-}$ P14 MPECs (sorted 2-weeks post-infection with LCMV). Gene expression in SLEC populations, sorted and analyzed at the same time, also showed minimal

differences between WT and *P2rx7*$^{-/-}$ groups (data not shown). **(c–g)**, at day 8 **(c,e–f)** or 14d **(d,g)**, splenic WT and *P2rx7*$^{-/-}$ MPEC and SLEC subpopulations were stained for MTG **(c)**, Cox-IV **(d)** TMRE **(e)** or for 2-NBDG uptake **(f,g)**; two independent experiments, n=4–5 from all experiments. In **(h)**, the ECAR levels in MPECs and SLECs (from the experiments described in Fig. 2d–f) are shown (three independent experiments, n=8–12). In **i–l**, 4-weeks following priming with LCMV, WT and *P2rx7*$^{-/-}$ P14 CD8^{+} T_{CM} and T_{EM} subsets were assessed for expression of Cox-IV **(i)**, Glut1 **(j)** or CPT1a **(l)**, or uptake of the dye Bodipy **(k)**. In **(j–l)**, representative flow cytometric plots are shown for T_{CM} populations (relative to naïve WT host CD8^{+} T cells) on the left, and average median different in staining relative to naïve WT host CD8^{+} T cells. (**i–l**) Three independent experiments, n=5–10 from all experiments. **(a,c–l)** mean ± SEM is shown; **(a,c,e–l)** Two-tailed Student's t-test; **(d)** One-way ANOVA with Tukey's post-test; *P≤0.05, **P≤0.01, ***P≤0.001.

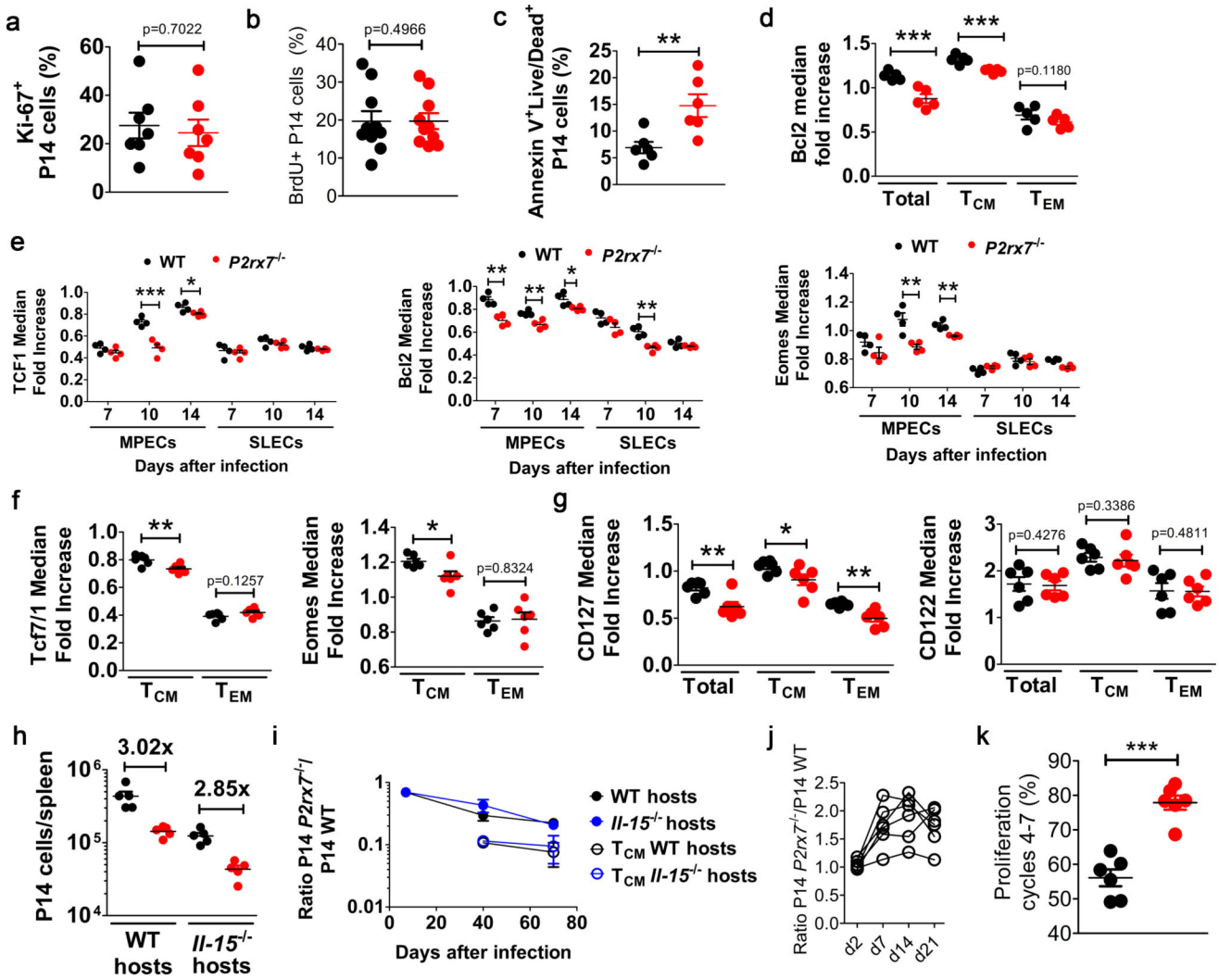

Ext. Data Fig. 4. P2RX7 signaling is required for survival rather than homeostatic proliferation of long-lived memory CD8^{+} T cells

(a–g) WT (black) and *P2rx7*$^{-/-}$ (red) P14 CD8^{+} T cells were mixed 1:1, co-adoptively transferred into B6.SJL mice that were subsequently infected with LCMV, and donor cells

identified as in Fig. 1 (data from three independent experiments, n=4–10 from all experiments). **(a–d)** the percentage of Ki-67$^+$ cells (*ex vivo* staining; **a**), BrdU$^+$ cells **(b)**, Annexin V$^+$ Live/Dead$^+$ cells **(c)**, and Bcl2 median fold increase (relative to median values of naïve CD8$^+$ T cells) for bulk, T_{CM} and T_{EM} subsets **(d)** was determined for WT (black) and *P2rx7*$^{-/-}$ (red) P14 CD8$^+$ T cells 8-weeks post-infection (same color scheme used throughout figure). **(e)** shows median fold increase (relative to naïve CD8$^+$ T cells) for expression of Tcf1 (left), Bcl2 (center) and Eomes (right) in MPECs and SLECs WT and *P2rx7*$^{-/-}$ P14 CD8$^+$ T cells at the indicated times. In **(f),** expression of Tcf1 (left) and Eomes (right) (shown as median expression relative to naïve CD8$^+$ T cells) was determined in in splenic T_{EM} and T_{CM} subsets of WT and *P2rx7*$^{-/-}$ P14 CD8$^+$ T cells, 4-weeks post-infection). In **(g),** CD127 (left) and CD122 (right) median expression (relative to naïve CD8$^+$ T cells) for splenic bulk, T_{CM} and T_{EM} subsets was determined 4-weeks post-infection. **(h,i)**, WT and *P2rx7*$^{-/-}$ P14 CD8$^+$ T cells were mixed 1:1 and co-adoptively transferred into B6.SJL or IL-15$^{-/-}$ mice, subsequently infected with LCMV (data from two independent experiments, n=4–5 from all experiments). **(h)** shows numbers of WT and *P2rx7*$^{-/-}$ P14 CD8$^+$ T cells in each host (4-weeks post-infection). **(i)** Ratio of total and T_{CM} *P2rx7*$^{-/-}$ to WT P14 CD8$^+$ T cells in spleens from WT and IL-15$^{-/-}$ hosts at indicated times post-infection. **(j,k)**, Congenically distinct WT and *P2rx7*$^{-/-}$ P14 CD8$^+$ T cells were stained with CFSE, mixed 1:1 and co-adoptively transferred into *Rag2*$^{-/-}$ mice. Data from 2 independent experiments, n=6 total. **(j)** Ratio of *P2rx7*$^{-/-}$ to WT P14 CD8$^+$ T cells in the blood of *Rag2*$^{-/-}$ hosts at indicated times post-transfer. **(k)**, Percentages of *P2rx7*$^{-/-}$ and WT P14 CD8$^+$ T cells proliferating over 4 cycles in spleens of *Rag2*$^{-/-}$ hosts 3 weeks post-transfer. **(a–k)** mean ± SEM is shown. **(a–d,f–h,k)**, Two-tailed Student's t-test; **(e)** Two-way ANOVA with Bonferroni post-test; *P≤0.05, **P≤0.01, ***P≤0.001.

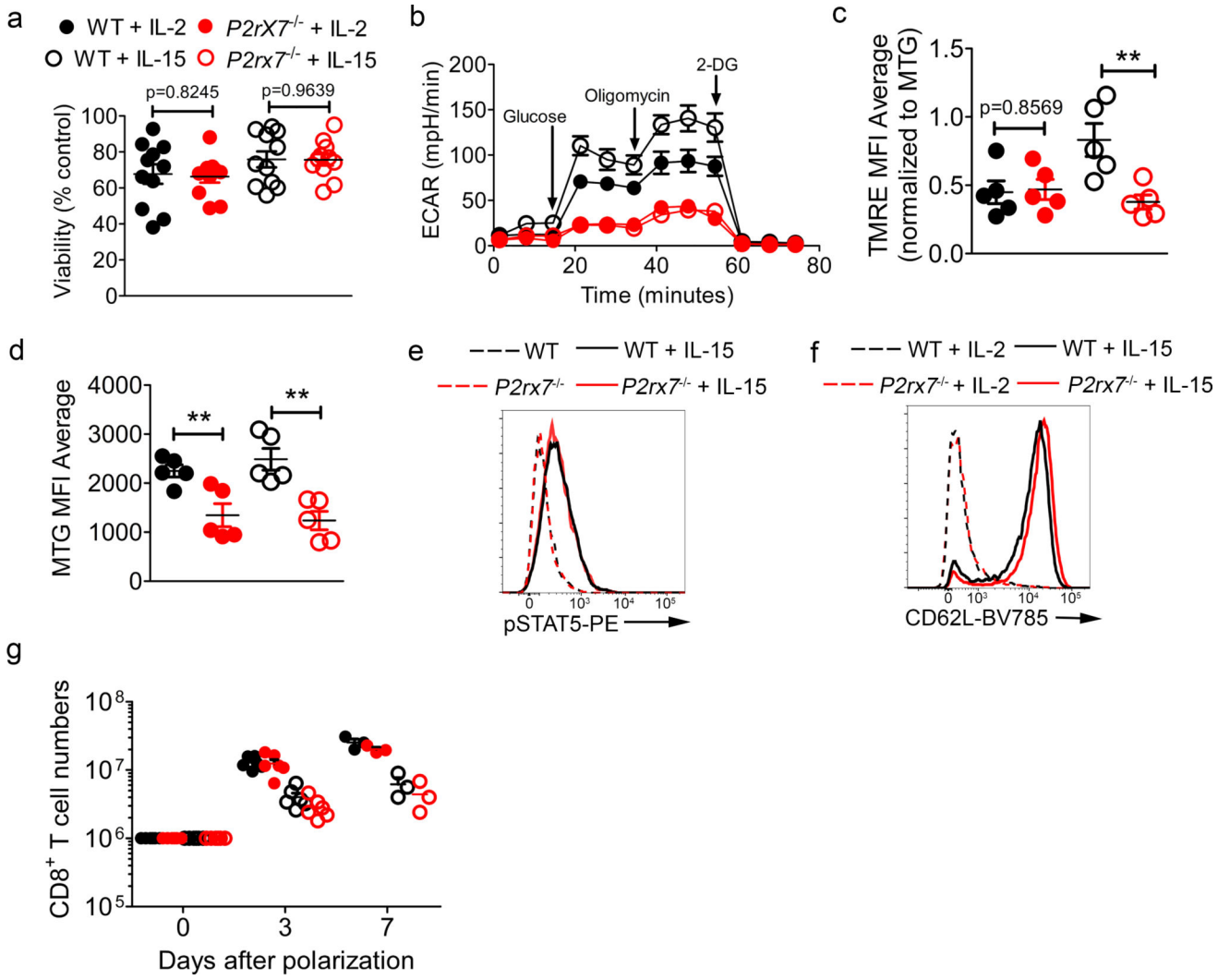

Ext. Data Fig. 5. Defective metabolism of IL-15-polarized CD8$^+$ T cells in the absence of P2RX7

(a), Viability of WT and *P2rx7*$^{-/-}$ P14 cells maintained under culture conditions used for extracellular flux assays for 4h (data from two independent experiments, n=11 from all experiments). The same color scheme is used throughout the figure. **(b–d)**, WT or *P2rx7*$^{-/-}$ P14 cells were *in vitro*-activated and subsequently polarized in IL-2 or IL-15 for 72h and assayed for extracellular acidification rate ("ECAR") to measure aerobic glycolysis **(b)**; uptake of the dye TMRE to measure mitochondrial membrane potential (data normalized to MTG staining) **(c)**; staining with MTG to determined total mitochondrial mass **(d)**. **(b–d)** Data from three independent experiments, n=5–6 from all experiments). **(e)**, WT and *P2rx7*$^{-/-}$ P14 cells were activated *in vitro* for 72h, then stimulated with IL-15 (or not) for 30 min and immediately assayed for pSTAT5 expression. Data are representative of two independent experiments (n=6 total). **(f),** WT and *P2rx7*$^{-/-}$ P14 cells were activated *in vitro* for 72h, then stimulated with IL-15 or IL-2 for 72h and assayed for expression of CD62L. Data are representative of three independent experiments (n=6 total). **(g),** Numbers of viable WT and *P2rx7*$^{-/-}$ P14 cells following activation and subsequent culture in IL-15 or IL-2 for the indicated number of days. Values for WT and *P2rx7*$^{-/-}$ cells were not significantly

different (i.e. all p values were >0.05). Data from three independent experiments (n=3–6 total). **(a–d,g)** mean ± SEM is shown; **(a,c–d,g);** Two-tailed Student's t-test; **P≤0.01.

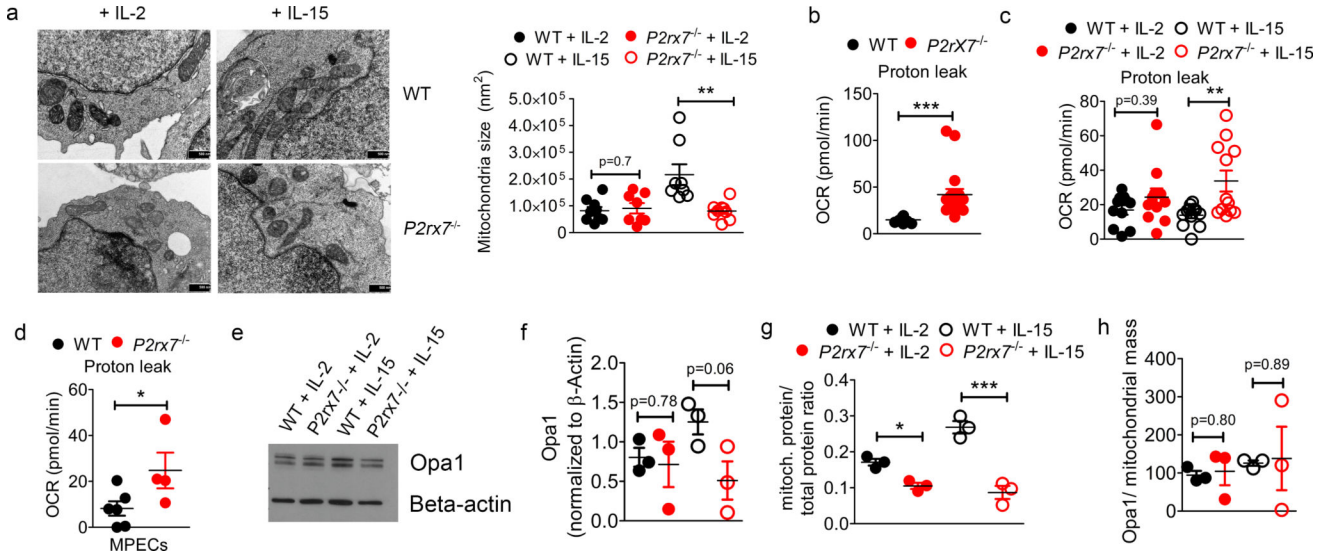

Ext. Data Fig. 6. P2RX7 controls mitochondrial integrity in CD8$^+$ T cells during immune responses

(a), Representative electron micrographs showing mitochondrial structures (left) and mitochondrial area measurements (right) of *in vitro*-activated WT and *P2rx7*$^{-/-}$ P14 cells following culture for 72h in IL-2 or IL-15 as indicated. Representative of 3 independent experiments (n=8–9 in total). Black bars indicate 500nm. **(b,c)**, WT and *P2rx7*$^{-/-}$ P14 cells were activated *in vitro* for 72h and assayed at that time **(b)** or after a further 72h culture in IL-2 or IL-15 (as in Fig. 3b) **(c)** and oxygen consumption rate measured. Graphs show values for proton leak (i.e. the difference in OCR values after oligomycin and after Antimycin A/rotenone addition – see Fig. 3b for details of inhibitor addition). Data are from three independent experiments (n=11–18 total). (**d**) calculated proton leak derived from OCR measurements on *in vivo* activated WT and *P2rx7*$^{-/-}$ P14 CD8$^+$ MPEC described in Fig. 2d–f (data from three independent experiments, data pooled from 5 mice per experiment; n=4–6 wells in total). **(e–h)** WT and *P2rx7*$^{-/-}$ P14 cells were activated *in vitro* and polarized with either IL-2 or IL-15 (as in Fig. 3b); total cell **(e,f,g)** and mitochondrial **(g,h)** protein extracts were collected for protein quantification experiments. Data from three independent experiments, samples pooled from n=6 mice total (2 mice per experiment). **(e)** Representative blot showing Opa1 expression in polarized WT or *P2rx7*$^{-/-}$ P14 cells, in comparison with beta-actin (For gel source data, see Supplementary Figure 1). **(f)** Opa1 protein levels in polarized WT or *P2rx7*$^{-/-}$ P14 cells, normalized to beta-actin. **(g)** mitochondrial concentration (normalized by total protein concentration) in polarized WT or *P2rx7*$^{-/-}$ P14 cells. **(h)** Opa1 protein levels in polarized WT or *P2rx7*$^{-/-}$ P14 cells, normalized to total mitochondrial concentration. **(a–d,f–h)**, mean ± SEM is shown; **(a–b,d)** Two-tailed Student's t-test; **(c, f–h)** Two-sided Mann-Whitney's test; *P≤0.05, **P≤0.01, ***P≤0.001.

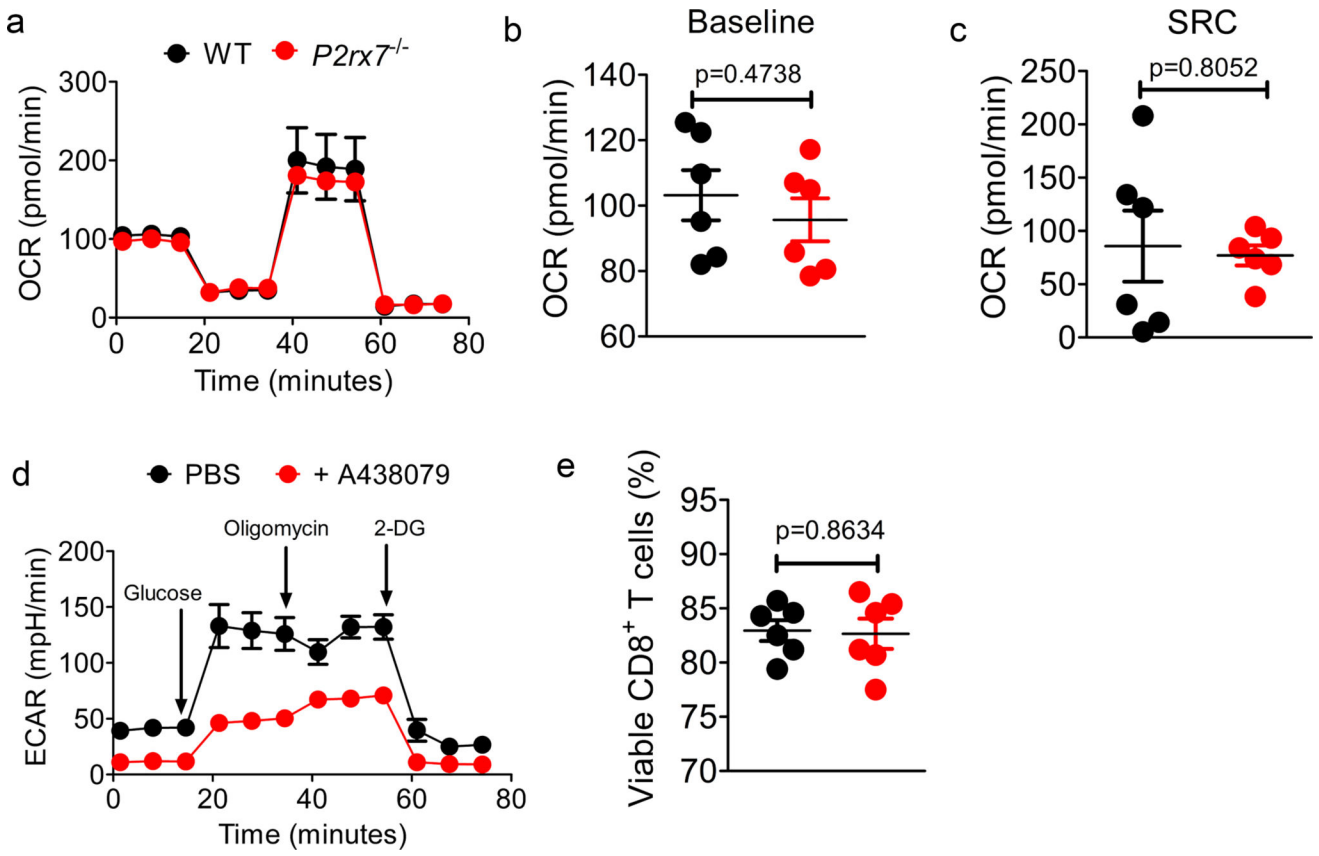

Ext. Data Fig. 7. Normal metabolic function of *P2rx7*$^{-/-}$ naïve P14 CD8^{+} T cells, while pharmacological inhibition of P2RX7 compromises aerobic glycolysis of *in vitro* activated CD8^{+} T cells

(a–c), Naïve WT and *P2rx7*$^{-/-}$ P14 cells were isolated and evaluated for different metabolism parameters (data from three independent experiments, n=6 total). **(d,e),** Human CD8^{+} T cells were *in vitro* activated in the presence of the P2RX7 inhibitor A-438079 (red) or vehicle alone (black) (from 20h of the beginning of the activation cultures), and assessed for extracellular acidification rate ("ECAR") **(d)** or for viability of cells cultured in parallel under the same conditions used for extracellular flux assays **(e)**. **(d–e)** Data are from three independent experiments, n=4–6 from all experiments. **(a–e)** mean ± SEM is shown; **(b–c,e)**, Two-tailed Student's t-test.

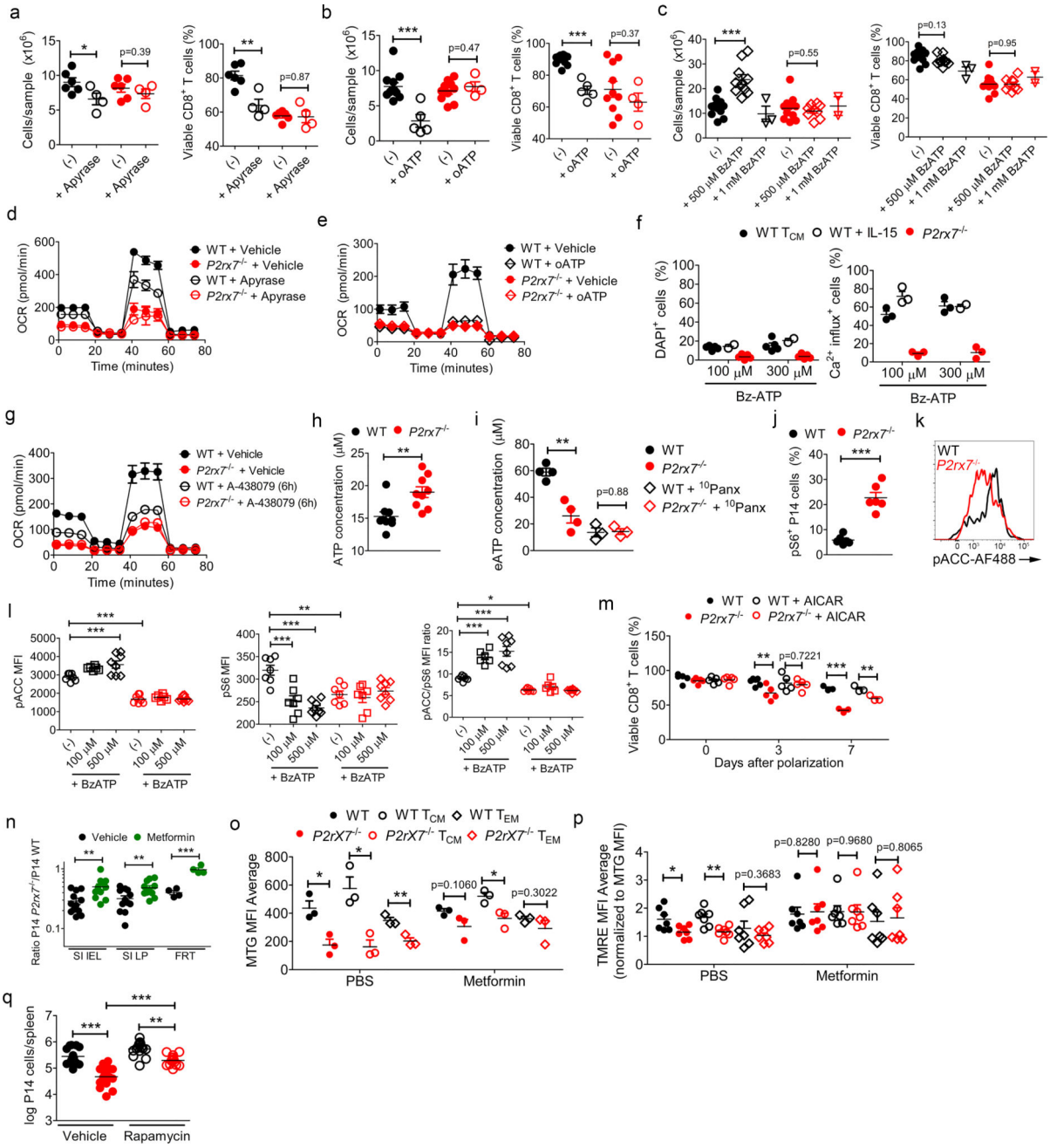

Ext. Data Fig. 8. P2RX7-mediated eATP sensing is crucial for optimal CD8$^+$ T cell immunometabolism via AMPK/mTOR pathway regulation

(a–g), WT and *P2rx7*$^{-/-}$ P14 cells were *in vitro* activated and polarized with IL-15 (as in Fig. 3b). Data from three independent experiments, samples pooled from n=6 mice per experiment; n=3–12 total samples. **(a–c)** show the numbers of P14 cells (left) and viability (right) in cultures supplemented with **(a)** the eATP hydrolytic enzyme Apyrase, **(b)** the inhibitor oATP or **(c)** the eATP analog BzATP, during cell culture. In **(d,e,g)** IL-15-polarized WT or *P2rx7*$^{-/-}$ P14 cells were assayed for OCR 1h after addition of apyrase **(d)** or oATP **(e)**, or 6h after addition of A-438079 **(g)**. In **(f)**, IL-15-polarized cells or *ex vivo* WT P14

T_{CM} (isolated 4w after LCMV infection) were incubated with either DAPI (left) or Indo-1 (right) and stimulated with the indicated concentrations of Bz-ATP during kinetic flow cytometric analysis. The percentage of cells showing DAPI uptake (left) or Ca^{2+} influx (right) over 30m are shown. **(f)** Data from two independent experiments, samples pooled from n=5 mice total; n=2–5 samples. In **(h)**, *in vitro*-activated (72h) WT and *P2rx7*$^{-/-}$ P14 cells were assayed for intracellular ATP concentrations. Data from three independent experiments, n=9 total. In **(i),** *In vitro*-activated, IL-15 polarized (24h post-polarization) WT or *P2rx7*$^{-/-}$ P14 cells were assayed for extracellular ATP concentration, following culture without or with the Panx1 inhibitor ^{10}Panx. Data from two independent experiments, n=3–4 total samples (pooled from 6 mice). **(j)**, WT and *P2rx7*$^{-/-}$ P14 cells were co-adoptively transferred and assayed 4w post LCMV infection (as in Fig. 1a) and the *ex vivo* frequency of pS6-expressing cells determined by flow cytometry. Data are from two independent experiments (n=6 total). **(k)** Representative histograms showing expression of pACC in IL-15-polarized WT (black) and *P2rx7*$^{-/-}$ (red) P14 cells (relative to Fig. 3l; representative from three independent experiments, n=6 total). **(l)** *In vitro* activated and IL-15-polarized WT and *P2rx7*$^{-/-}$ P14 cells were cultured for 6h with the indicated concentrations of BzATP then stained for pACC (left) and pS6 (center) and the pACC/pS6 ratio was determined (right). Data from three independent experiments, n=6–8 total. **(m)** *In vitro*-activated WT and *P2rx7*$^{-/-}$ P14 cells were IL-15 polarized in presence or absence of the AMPK activator AICAR as in Fig. 3l. The percentage of viable cells at the indicated times following initiation of IL-15 +/− AICAR culture is indicated. Data are from three independent experiments (n=3–6 total; samples pooled from n=6 mice total). **(n–p)** WT and *P2rx7*$^{-/-}$ P14 $CD8^+$ T cells were mixed 1:1, co-adoptively transferred into B6.SJL mice that were subsequently infected with LCMV, and donor cells identified as in Fig. 1. The animals were treated with Metformin or PBS control during the first week of LCMV infection, and the cells analyzed at day 30. Data are compiled from three independent experiments (n=11–12 total, n=4 for FRT samples). Panel **(n)** relates to Fig. 3m and shows *P2rx7*$^{-/-}$ /WT P14 ratio in indicated non-lymphoid tissues (n=9 except female reproductive tract – FRT – where n=4). **(o,p)** shows measurements of mitochondrial mass (measured by MTG) **(o)** and mitochondrial membrane potential (measured by TMRE staining, normalized to MTG staining) **(p)** for indicated splenocyte subsets (n=3–6 total samples). **(q)** WT and *P2rx7*$^{-/-}$ P14 $CD8^+$ T cells were mixed 1:1, co-adoptively transferred into B6.SJL mice that were subsequently infected with LCMV, and donor cells identified as in Fig. 1. The animals were treated with Rapamycin or PBS control between days 4–8 post-LCMV infection, and the cells analyzed at day 30. The numbers of WT or *P2rx7*$^{-/-}$ P14 cells are shown (log-transformed values). Data are compiled from three independent experiments (n=15 total). **(a–j,l–q)**, mean ± SEM is shown; **(a–c,h–j,m–p)** Two-tailed Student's t-test; **(l,q)** One-way ANOVA with Tukey's post-test; *P≤0.05, **P≤0.01, ***P≤0.001.

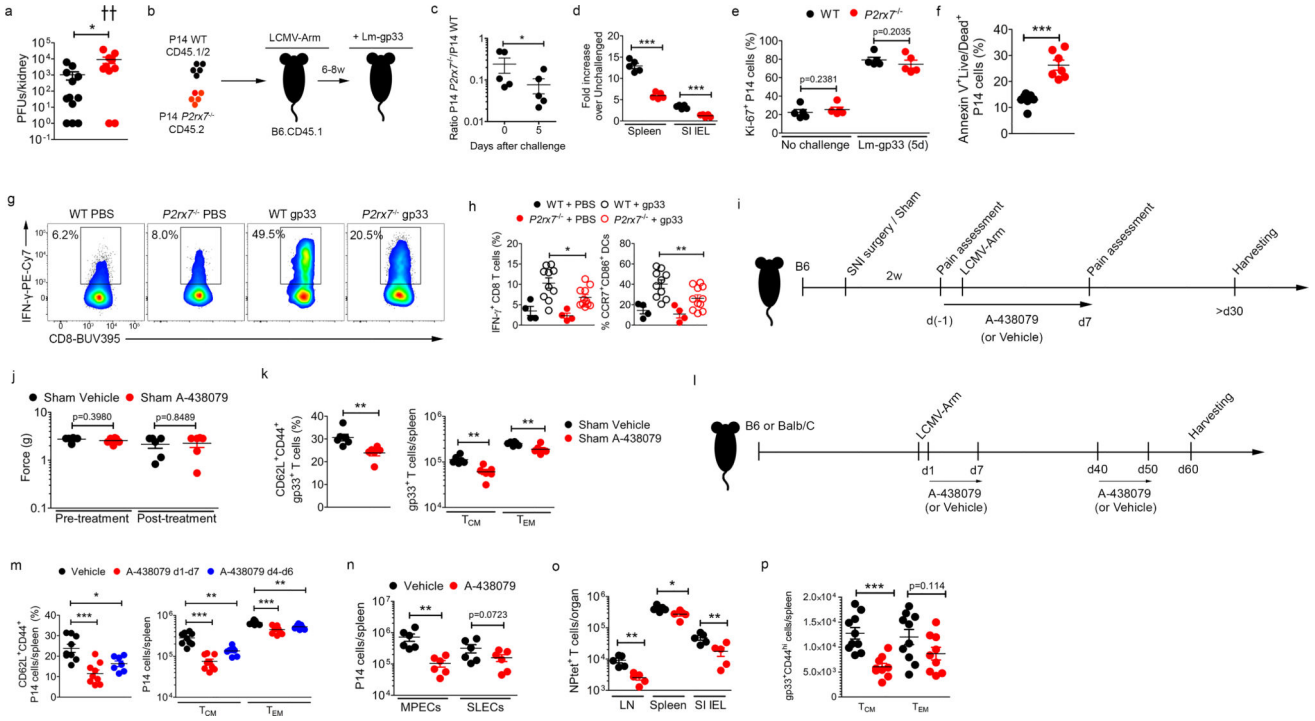

Ext. Data Fig. 9. P2RX7 deficiency compromises memory CD8$^+$ T cell function, and P2RX7 pharmacological blockade impairs generation of CD8$^+$ T cell memory cells *in vivo*

(a), WT or *P2rx7*$^{-/-}$ mice were infected with LCMV-Cl13, and the PFU levels in the kidneys were quantified 4 weeks post-infection. Data from three independent experiments, n=7 total. **(b–f),** WT and *P2rx7*$^{-/-}$ P14 CD8$^+$ T cells were mixed 1:1, co-adoptively transferred into B6.SJL mice that were subsequently infected with LCMV then challenged (or not) with Lm-gp33 6–8 weeks later **(b)**. Data are from two independent experiments (n=5–7 total). **(c)** shows *P2rx7*$^{-/-}$/WT splenic P14 CD8$^+$ T cell ratio before (0d) and post-challenge (5d), while **(d)** shows fold-increase in numbers of WT or *P2rx7*$^{-/-}$ P14 cells in indicated tissues, relative to mice that did not receive Lm-gp33 challenge. The percentage of cells in cell cycle was determined by Ki-67 staining **(e)**, and the frequency of dying cells indicated by the percentage of Annexin V$^+$L/D$^+$ cells in mice 5d following Lm-gp33 challenge **(f)**. **(g–h)** WT and *P2rx7*$^{-/-}$ P14 CD8$^+$ T cells were individually transferred into B6.SJL mice that were subsequently infected with LCMV. At 6–8-weeks, the mice were transcervically challenged with gp33 or PBS as in Fig. 4d. **(g)** Flow cytometry plots for IFN-γ production by WT or *P2rx7*$^{-/-}$ P14 in PBS or gp33-treated mice **(h)** Percentage of IFN-γ$^+$ "bystander" (i.e. non-P14) CD8$^+$ T cells (left) and the percentage of CCR7$^+$CD86$^+$ DCs (right) in the FRT 12h later. **(g–h)** Data are from three independent experiments, n=4–11 total). **(i–k)**, Schematic of experimental scheme combining spare nerve injury (SNI), LCMV infection and A-438079 treatment **(i)**. For surgery, two of the three branches of the sciatic nerve in one hind limb were exposed and cut (SNI – see Fig 4)) or left uncut (sham). After 2-weeks recovery from surgery, mice were assays for pain sensitivity, then infected with LCMV with or without A-438079 treatment for the first week post-infection. Mice were assayed again for pain sensitivity (day 7) and subsequent development of central (CD62L$^+$) and effector (CD62L$^-$) memory cells specific for the LCMV epitope gp33 (>day 30). Data are compiled from two

independent experiments, n=6 from all experiments. **(j)** shows pain sensitivity of sham-surgery mice (pre- and post-treatment) while **(k)** shows percentages of gp33-specific T_{CM} (left) and numbers of gp33-specific T_{CM} and T_{EM} (right) in sham surgery animals. **(l–p)**, In other studies, B6 or Balb/C mice were adoptively transferred or not with WT P14 cells, infected with LCMV, and treated with A-438079 in the time frames indicated, relative to infection. Data from 2–3 independent experiments, n=5–10 total. In **(m)**, Percentages of $CD62L^+CD44^+$ (T_{CM}) P14 cells/spleen (left) and spleen P14 T_{CM} and T_{EM} numbers (right) from the different treatment groups at 4-weeks post-infection were assessed. In **(n)**, P14 recipient mice were treated with PBS or A-438079 for the first week following LCMV infection, then assayed at 3-weeks for numbers of MPEC and SLEC populations. In **(o)**, Balb/C mice were infected with LCMV, treated with A-438079 throughout the first week post-infection, and the numbers of LCMV-specific ("$NPtet^+$") $CD8^+$ T cells were quantified in the spleen, lymph nodes and SI-IEL at 4 weeks post-infection. In **(p)**, B6 mice infected with LCMV were treated with A-438079 between days 40–50 post-infection and the numbers of $gp33^+$ $CD8^+$ T cells (T_{CM} and T_{EM}) per spleen were quantified at 8 weeks post-infection. **(a,c–f,h,j–k,m–p)** mean ± SEM is shown; **(a,c–f,k,n–p)**, Two-tailed Student's t-test; **(j)**, Two-sided Mann-Whitney's test; **(h,m)**, One-way ANOVA with Tukey's post-test; *P≤0.05, **P≤0.01, ***P≤0.001.

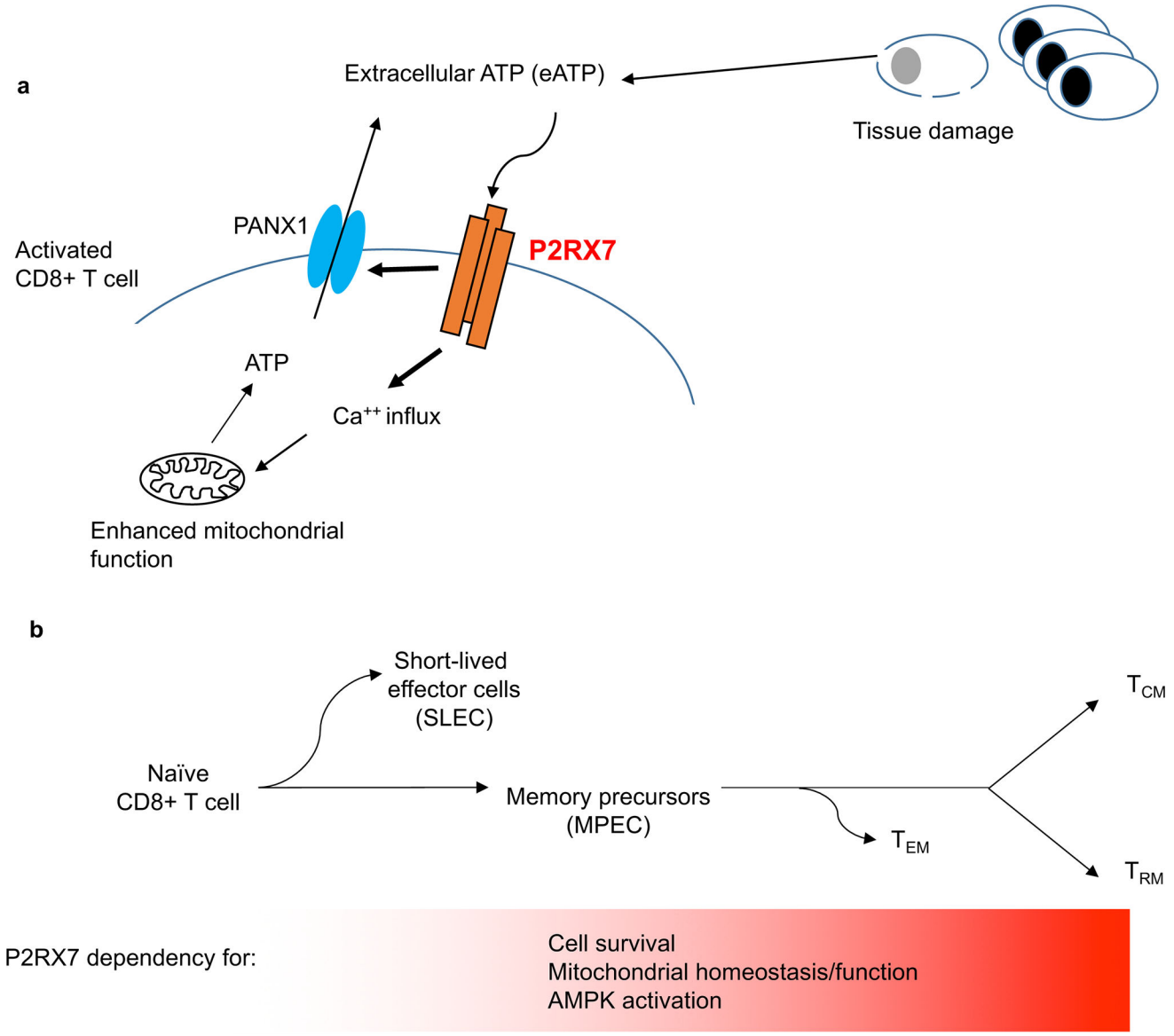

Ext. Data Fig. 10. Model of P2RX7 function in regulating long-lived CD8$^+$ T cell memory

(**a**) Following CD8$^+$ T cell activation, P2RX7 is stimulated by eATP (derived from damaged cells or exported from live activated cells). This induces calcium influx, increased mitochondrial metabolic activity, and activation of the ATP export channel PANX1 (bold arrows). Generation of eATP through PANX1 sustains P2RX7 activation, further promoting mitochondrial function and T cell homeostasis. (**b**) illustrates that the impact of P2RX7 function is magnified as the CD8$^+$ T cell response progresses into memory phase, with P2RX7 deficiency having little effect on effector T cells, while severely compromising survival and metabolic function in memory T cells, impairing the generation of long-lived central memory (T_{CM}) and CD103^{hi}/CD69^{hi} resident memory (T_{RM}) populations. P2RX7 activation is proposed to stimulate AMPK activation, which may arise from both calcium influx and increased AMP/ATP ratios as a result of P2RX7/PANX1 activity. A requirement for eATP stimulation of P2RX7 persists throughout memory CD8+ T cell maintenance.

Supplementary Material

Refer to Web version on PubMed Central for supplementary material.

Acknowledgments

We thank the UMN Flow Cytometry Resource for cell sorting, Dr. Christine Henzler (UMN Supercomputing Institute) for bioinformatics analysis, Dr. Fang Zhou (UMN Characterization Facility) for transmission electron microscopy, Mark Pierson for viral plaque assays and the NIH Tetramer Core for peptide/MHC tetramers. We thank Ananda Goldrath, Susan Kaech, Gerry Shadel, Russell Jones, Erica Pearce, Marc Jenkins, Vaiva Vezys and members of the Jamequist lab and UMN Center for Immunology for insightful discussions. The UMN Characterization Facility is a member of the NSF-funded Materials Research Facilities Network (www.mrfn.org) via the MRSEC program. This work was supported by NIH grants AI38903 and AI75168 (S.C.J.), CA157971 (A.K.), and MN Partnership Infrastructure Award MNPIF#16.09 (A.K.). H.B.dS. was supported by a CNPq research fellowship, from the Ministry of Science, Technology and Innovation of Brazil.

References

1Heil M, Land WG. Danger signals - damaged-self recognition across the tree of life. Front Plant Sci. 2014; 5:578. [PubMed: 25400647]

2Surprenant A, Rassendren F, Kawashima E, North RA, Buell G. The cytolytic P2Z receptor for extracellular ATP identified as a P2X receptor (P2X7). Science. 1996; 272:735–738. [PubMed: 8614837]

3Chessell IP, et al. Disruption of the P2X7 purinoceptor gene abolishes chronic inflammatory and neuropathic pain. Pain. 2005; 114:386–396. DOI: 10.1016/j.pain.2005.01.002 [PubMed: 15777864]

4Mariathasan S, et al. Cryopyrin activates the inflammasome in response to toxins and ATP. Nature. 2006; 440:228–232. DOI: 10.1038/nature04515 [PubMed: 16407890]

5Williams MA, Bevan MJ. Effector and memory CTL differentiation. Annu Rev Immunol. 2007; 25:171–192. [PubMed: 17129182]

6Schenkel JM, Masopust D. Tissue-resident memory T cells. Immunity. 2014; 41:886–897. DOI: 10.1016/j.immuni.2014.12.007 [PubMed: 25526304]

7Di Virgilio F, Dal Ben D, Sarti AC, Giuliani AL, Falzoni S. The P2X7 Receptor in Infection and Inflammation. Immunity. 2017; 47:15–31. DOI: 10.1016/j.immuni.2017.06.020 [PubMed: 28723547]

8Rissiek B, Haag F, Boyer O, Koch-Nolte F, Adriouch S. P2X7 on Mouse T Cells: One Channel, Many Functions. Front Immunol. 2015; 6:204. [PubMed: 26042119]

9Proietti M, et al. ATP-gated ionotropic P2X7 receptor controls follicular T helper cell numbers in Peyer's patches to promote host-microbiota mutualism. Immunity. 2014; 41:789–801. DOI: 10.1016/j.immuni.2014.10.010 [PubMed: 25464855]

10Trautmann A. Extracellular ATP in the immune system: more than just a "danger signal". Sci Signal. 2009; 2:pe6. [PubMed: 19193605]

11Utzschneider DT, et al. T Cell Factor 1-Expressing Memory-like CD8(+) T Cells Sustain the Immune Response to Chronic Viral Infections. Immunity. 2016; 45:415–427. DOI: 10.1016/j.immuni.2016.07.021 [PubMed: 27533016]

12Im SJ, et al. Defining CD8+ T cells that provide the proliferative burst after PD-1 therapy. Nature. 2016; 537:417–421. DOI: 10.1038/nature19330 [PubMed: 27501248]

13He R, et al. Follicular CXCR5- expressing CD8(+) T cells curtail chronic viral infection. Nature. 2016; 537:412–428. DOI: 10.1038/nature19317 [PubMed: 27501245]

14Pearce EL, Poffenberger MC, Chang CH, Jones RG. Fueling immunity: insights into metabolism and lymphocyte function. Science. 2013; 342:1242454. [PubMed: 24115444]

15van der Windt GJ, et al. Mitochondrial respiratory capacity is a critical regulator of CD8+ T cell memory development. Immunity. 2012; 36:68–78. DOI: 10.1016/j.immuni.2011.12.007 [PubMed: 22206904]

16Buck MD, O'Sullivan D, Pearce EL. T cell metabolism drives immunity. J Exp Med. 2015; 212:1345–1360. DOI: 10.1084/jem.20151159 [PubMed: 26261266]

17Ledderose C, et al. Mitochondrial Dysfunction, Depleted Purinergic Signaling, and Defective T Cell Vigilance and Immune Defense. J Infect Dis. 2016; 213:456–464. DOI: 10.1093/infdis/jiv373 [PubMed: 26150546]

18Schenk U, et al. Purinergic control of T cell activation by ATP released through pannexin-1 hemichannels. Sci Signal. 2008; 1:ra6. [PubMed: 18827222]

19Chang JT, Wherry EJ, Goldrath AW. Molecular regulation of effector and memory T cell differentiation. Nat Immunol. 2014; 15:1104–1115. DOI: 10.1038/ni.3031 [PubMed: 25396352]

20Sprent J, Surh CD. Normal T cell homeostasis: the conversion of naive cells into memory-phenotype cells. Nat Immunol. 2011; 12:478–484. [PubMed: 21739670]

21Carrio R, Bathe OF, Malek TR. Initial antigen encounter programs CD8+ T cells competent to develop into memory cells that are activated in an antigen-free, IL-7- and IL-15-rich environment. J Immunol. 2004; 172:7315–7323. [PubMed: 15187107]

22Buck MD, et al. Mitochondrial Dynamics Controls T Cell Fate through Metabolic Programming. Cell. 2016; 166:63–76. DOI: 10.1016/j.cell.2016.05.035 [PubMed: 27293185]

23Donnelly-Roberts DL, Jarvis MF. Discovery of P2X7 receptor-selective antagonists offers new insights into P2X7 receptor function and indicates a role in chronic pain states. Br J Pharmacol. 2007; 151:571–579. DOI: 10.1038/sj.bjp.0707265 [PubMed: 17471177]

24Saez PJ, Vargas P, Shoji KF, Harcha PA, Lennon-Dumenil AM, Saez JC. ATP promotes the fast migration of dendritic cells through the activity of pannexin 1 channels and P2X7 receptors. Sci Signal. 2017; 10(506):aah7107.doi: 10.1126/scisignal.aah7107

25Blagih J, et al. The energy sensor AMPK regulates T cell metabolic adaptation and effector responses in vivo. Immunity. 2015; 42:41–54. DOI: 10.1016/j.immuni.2014.12.030 [PubMed: 25607458]

26Pearce EL, et al. Enhancing CD8 T-cell memory by modulating fatty acid metabolism. Nature. 2009; 460:103–107. DOI: 10.1038/nature08097 [PubMed: 19494812]

27Schenkel JM, et al. Resident memory CD8 T cells trigger protective innate and adaptive immune responses. Science. 2014

28Bartlett R, Stokes L, Sluyter R. The P2X7 receptor channel: recent developments and the use of P2X7 antagonists in models of disease. Pharmacol Rev. 2014; 66:638–675. DOI: 10.1124/pr.113.008003 [PubMed: 24928329]

29Matzinger P. Tolerance, danger, and the extended family. Annu Rev Immunol. 1994; 12:991–1045. DOI: 10.1146/annurev.iy.12.040194.005015 [PubMed: 8011301]

30Janeway CA Jr, Medzhitov R. Innate immune recognition. Annu Rev Immunol. 2002; 20:197–216. DOI: 10.1146/annurev.immunol.20.083001.084359 [PubMed: 11861602]

31Thompson EA, Beura LK, Nelson CE, Anderson KG, Vezys V. Shortened Intervals during Heterologous Boosting Preserve Memory CD8 T Cell Function but Compromise Longevity. J Immunol. 2016; 196:3054–3063. DOI: 10.4049/jimmunol.1501797 [PubMed: 26903479]

32Schenkel JM, Fraser KA, Vezys V, Masopust D. Sensing and alarm function of resident memory CD8(+) T cells. Nat Immunol. 2013; 14:509–513. DOI: 10.1038/ni.2568 [PubMed: 23542740]

33Sorge RE, et al. Genetically determined P2X7 receptor pore formation regulates variability in chronic pain sensitivity. Nature medicine. 2012; 18:595–599. DOI: 10.1038/nm.2710

34Pearce EL, et al. Enhancing CD8 T-cell memory by modulating fatty acid metabolism. Nature. 2009; 460:103–107. DOI: 10.1038/nature08097 [PubMed: 19494812]

35Araki K, et al. mTOR regulates memory CD8 T-cell differentiation. Nature. 2009; 460:108–112. DOI: 10.1038/nature08155 [PubMed: 19543266]

36Steinert EM, et al. Quantifying Memory CD8 T Cells Reveals Regionalization of Immunosurveillance. Cell. 2015; 161:737–749. DOI: 10.1016/j.cell.2015.03.031 [PubMed: 25957682]

37Skon CN, et al. Transcriptional downregulation of S1pr1 is required for the establishment of resident memory CD8+ T cells. Nat Immunol. 2013; 14:1285–1293. DOI: 10.1038/ni.2745 [PubMed: 24162775]

38Renkema KR, et al. IL-4 sensitivity shapes the peripheral CD8+ T cell pool and response to infection. J Exp Med. 2016; 213:1319–1329. DOI: 10.1084/jem.20151359 [PubMed: 27298446]

39Im SJ, et al. Defining CD8+ T cells that provide the proliferative burst after PD-1 therapy. Nature. 2016; 537:417–421. DOI: 10.1038/nature19330 [PubMed: 27501248]

40Daniels MA, Jameson SC. Critical role for CD8 in T cell receptor binding and activation by peptide/major or histocompatibility complex multimers. Journal of Experimental Medicine. 2000; 191:335–345. DOI: 10.1084/jem.191.2.335 [PubMed: 10637277]

41Anderson KG, et al. Intravascular staining for discrimination of vascular and tissue leukocytes. Nature protocols. 2014; 9:209–222. DOI: 10.1038/nprot.2014.005 [PubMed: 24385150]

42Schenkel JM, et al. IL-15-Independent Maintenance of Tissue-Resident and Boosted Effector Memory CD8 T Cells. J Immunol. 2016; 196:3920–3926. DOI: 10.4049/jimmunol.1502337 [PubMed: 27001957]

43Kieper WC, Jameson SC. Homeostatic expansion and phenotypic conversion of naive T cells in response to self peptide/MHC ligands. Proceedings of the National Academy of Sciences of the United States of America. 1999; 96:13306–13311. DOI: 10.1073/pnas.96.23.13306 [PubMed: 10557316]

44Buck MD, et al. Mitochondrial Dynamics Controls T Cell Fate through Metabolic Programming. Cell. 2016; 166:63–76. DOI: 10.1016/j.cell.2016.05.035 [PubMed: 27293185]

45van der Windt GJ, et al. Mitochondrial respiratory capacity is a critical regulator of CD8+ T cell memory development. Immunity. 2012; 36:68–78. DOI: 10.1016/j.immuni.2011.12.007 [PubMed: 22206904]

46Praetorius HA, Leipziger J. ATP release from non-excitable cells. Purinergic Signal. 2009; 5:433–446. DOI: 10.1007/s11302-009-9146-2 [PubMed: 19301146]

47Carrio R, Bathe OF, Malek TR. Initial antigen encounter programs CD8+ T cells competent to develop into memory cells that are activated in an antigen-free, IL-7- and IL-15-rich environment. J Immunol. 2004; 172:7315–7323. [PubMed: 15187107]

48Decosterd I, Woolf CJ. Spared nerve injury: an animal model of persistent peripheral neuropathic pain. Pain. 2000; 87:149–158. [PubMed: 10924808]

49Bourquin AF, et al. Assessment and analysis of mechanical allodynia-like behavior induced by spared nerve injury (SNI) in the mouse. Pain. 2006; 122:14 e11–14. DOI: 10.1016/j.pain.2005.10.036 [PubMed: 16542774]

50Chaplan SR, Bach FW, Pogrel JW, Chung JM, Yaksh TL. Quantitative assessment of tactile allodynia in the rat paw. J Neurosci Methods. 1994; 53:55–63. [PubMed: 7990513]

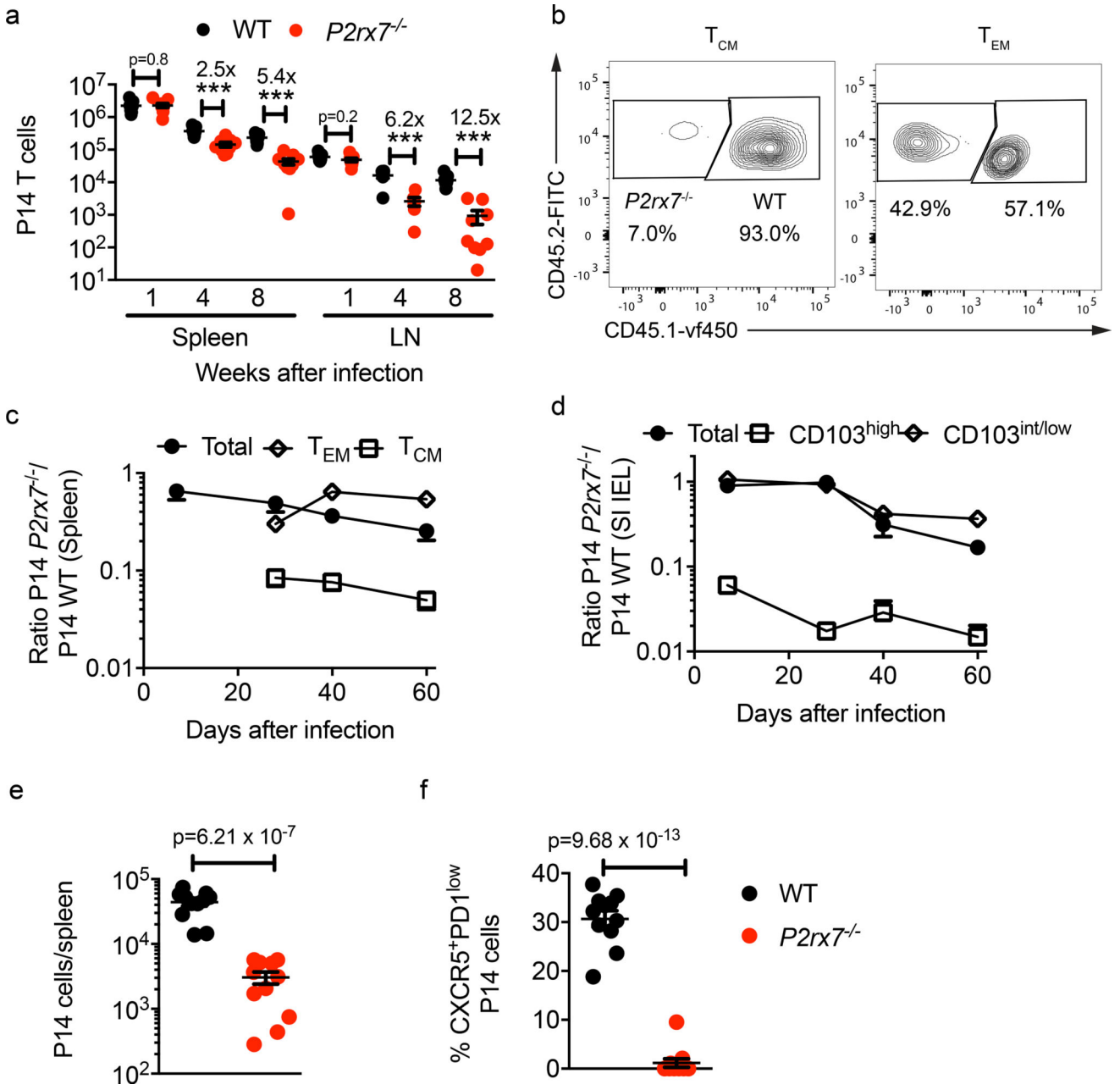

Fig. 1. P2RX7 is required for generation and maintenance of long-lived memory CD8$^+$ T cells

(a–d) WT and *P2rx7*$^{-/-}$ P14 were co-adoptively transferred and host mice infected with LCMV-Arm. **(a)** WT and *P2rx7*$^{-/-}$ P14 numbers in spleens and lymph nodes (LN). **(b)** Frequency of splenic WT and *P2rx7*$^{-/-}$ P14 T_{CM} and T_{EM} 8-weeks post-infection (representative of n=5). **(c,d)** *P2rx7*$^{-/-}$/WT P14 subset ratios in spleen **(c)** or small intestine intraepithelial lymphocytes (SI-IEL) **(d)**. **(e–f)** After WT and *P2rx7*$^{-/-}$ P14 cell co-adoptive transfer, mice were infected with LCMV-Cl13, and spleens analyzed 2–3 weeks later for donor cell numbers **(e)** and percentage CXCR5$^+$PD1^{low} **(f)**. **(a–f)** Mean ± SEM. **(a–d)** Three independent experiments, n=4–9 total. **(e–f)** Two independent experiments, n=11 total. **(a,e)** Two-tailed Student's t-test; **(f)**, Two-tailed Mann-Whitney test; **P≤0.01, ***P≤0.001.

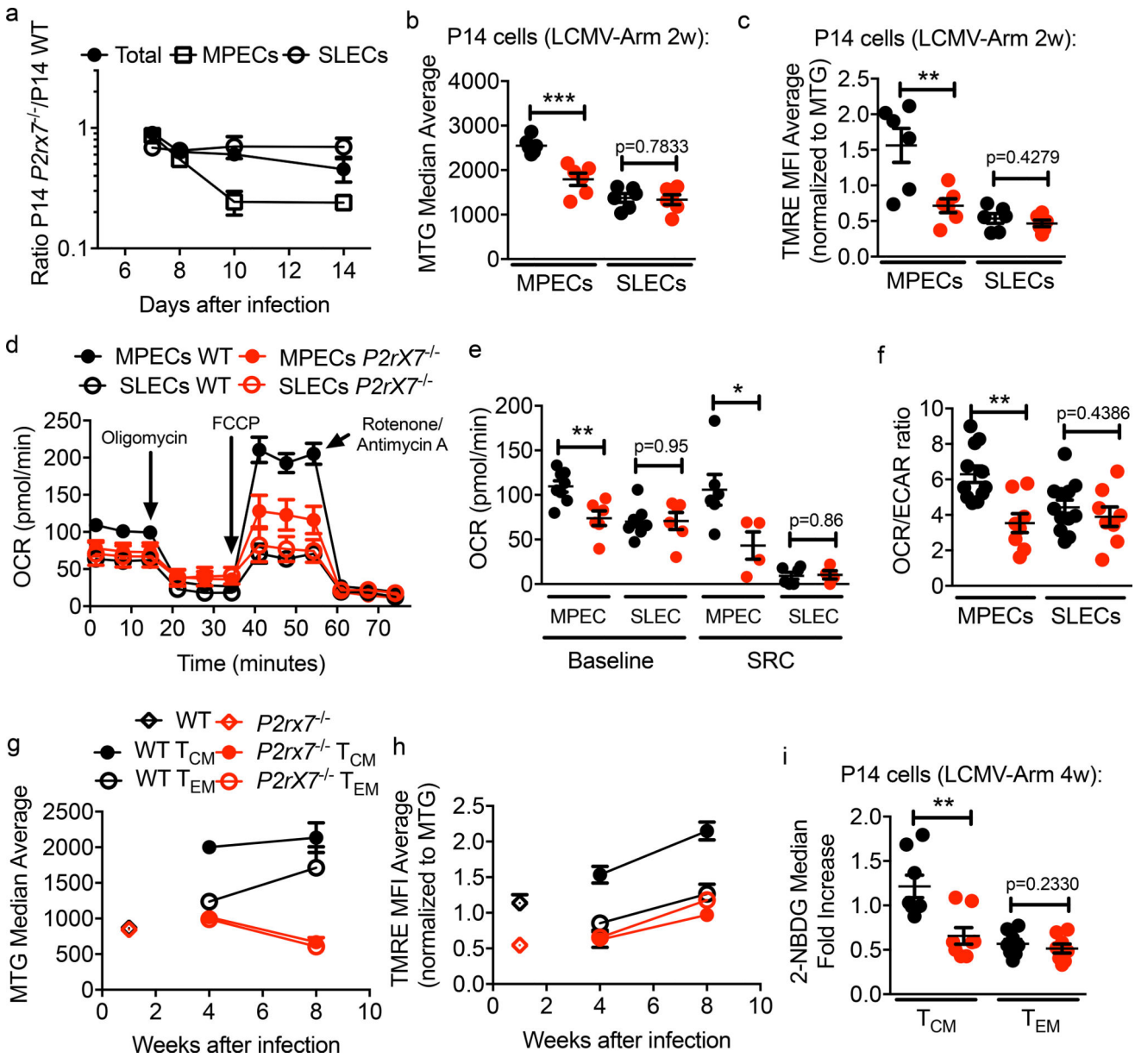

Fig. 2. P2RX7 regulates mitochondrial homeostasis in memory CD8$^+$ T cells

(a), *P2rx7*$^{-/-}$/WT P14 ratios among memory-precursor (MPEC) and short-lived (SLEC) effector cells. (**b,c**) Median fluorescence of Mitotracker Green (MTG) **(b)** and Tetramethylrhodamine (TMRE; normalized to MTG) **(c)** among MPEC and SLEC. **(d–f)**, Sorted WT and *P2rx7*$^{-/-}$ P14 MPEC and SLEC were analyzed for metabolic function, indicated by **(d,e)** oxygen consumption rate (OCR) parameters and **(f)** OCR/ECAR ratios. **(g–i)** subsets of splenic WT and *P2rx7*$^{-/-}$ P14 were stained for MTG **(g)** or TMRE **B** at indicated times. In **(i)**, median 2-NBDG uptake (relative to naïve CD8$^+$ T cells) in memory P14 subsets is shown. (**a–c,g–i**) Three independent experiments, n=5–6 total/timepoint. (**d–f**) Three independent experiments, cells pooled from 5 mice/experiment; n=4–6 total. **(a–i)** Mean ± SEM; **(b–c,f–h)**, Two-tailed Student's t-test; **(e,i)**, Two-tailed Mann-Whitney's test; *P≤0.05, **P≤0.01, ***P≤0.001.

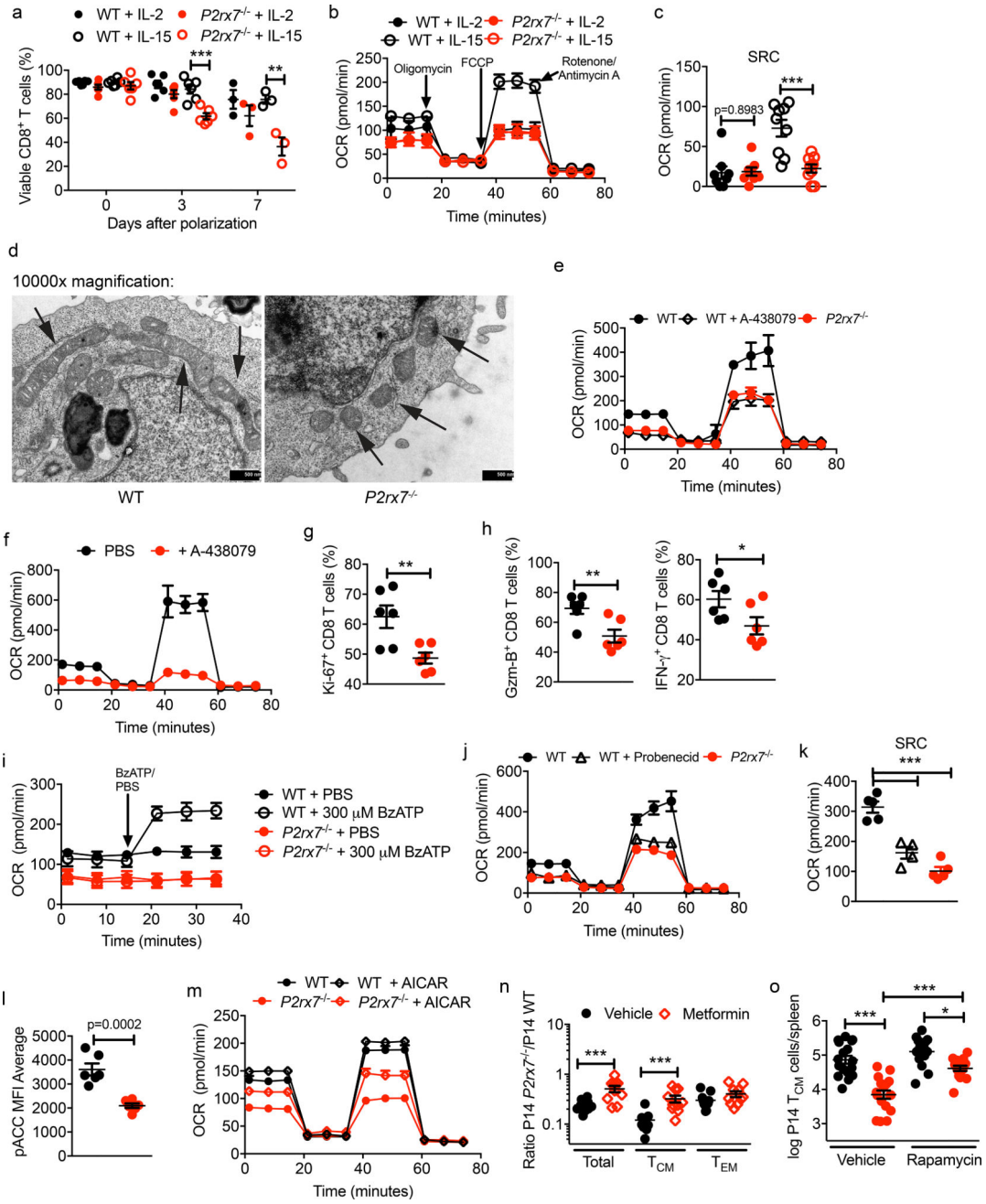

Fig. 3. P2RX7 ablation leads to aberrant metabolism and depressed AMPK activation in CD8$^+$ T cells

(a–d) *In vitro* activated WT and *P2rx7*$^{-/-}$ P14 were activated then polarized with IL-2 or IL-15 (cells pooled from 2 mice/experiment). **(a)** Cell viability during IL-2 or IL-15 cultures ($p \geq 0.2$ for all IL-2 polarized cells and IL-15 polarized at 24h). **(b,c)** OCR **(b)** and calculated SRC **(c)** for IL-2 or IL-15-polarized cells. **(d)** electron microscopy of mitochondria (arrows) in IL-15-polarized WT or *P2rx7*$^{-/-}$ P14 (black bars =500nm). **(e–k)** mouse **(e,i–k)** or human **(f–h)** CD8$^+$ T cells were stimulated *in vitro* in the presence of A-438079 **(e–h)**, BzATP **(i)**, Probenecid **(j,k)**, or vehicle controls. Mouse cells activated as in (**a**), human cells assayed

72h post-stimulation. OCR **(e,f,i,j)** and SRC **(k)** were measured and human cells assayed for proliferation (Ki67) **(g)** and Granzyme B/IFN-γ **(h). (l)** pACC in IL-15-polarized WT and *P2rx7*$^{-/-}$ P14 (representative flow cytometric histograms and median average values (right). In **(m)**, cells were incubated (6h) with/without AICAR prior to OCR measurement. **(n–o)** Mice receiving co-transferred WT and *P2rx7*$^{-/-}$ P14 were LCMV-infected primed and treated with metformin (1–7 dpi; **n)** or rapamycin (4–8 dpi; **o)**. *P2rx7*$^{-/-}$/WT ratios for splenic memory subsets **(n)** and P14 T_{CM} numbers were determined (**o**). **(a–o)** Three independent experiments, n=3–6 (**a**), 8–9 (**b–c**), 6 (**d,g–h,l–m**), 4–5 (**e,i**), 4 (**f**), 5–6 (**j–k**), 10–11 (**n**), 12–17 (**o**) total. **(a–c,e–o)** Mean ± SEM; **(a,c,g–h,l,n)**, Two-tailed Student's t-test; **(k,o)** One-way ANOVA + Tukey post-test, *P≤0.05, **P≤0.01, ***P≤0.001.

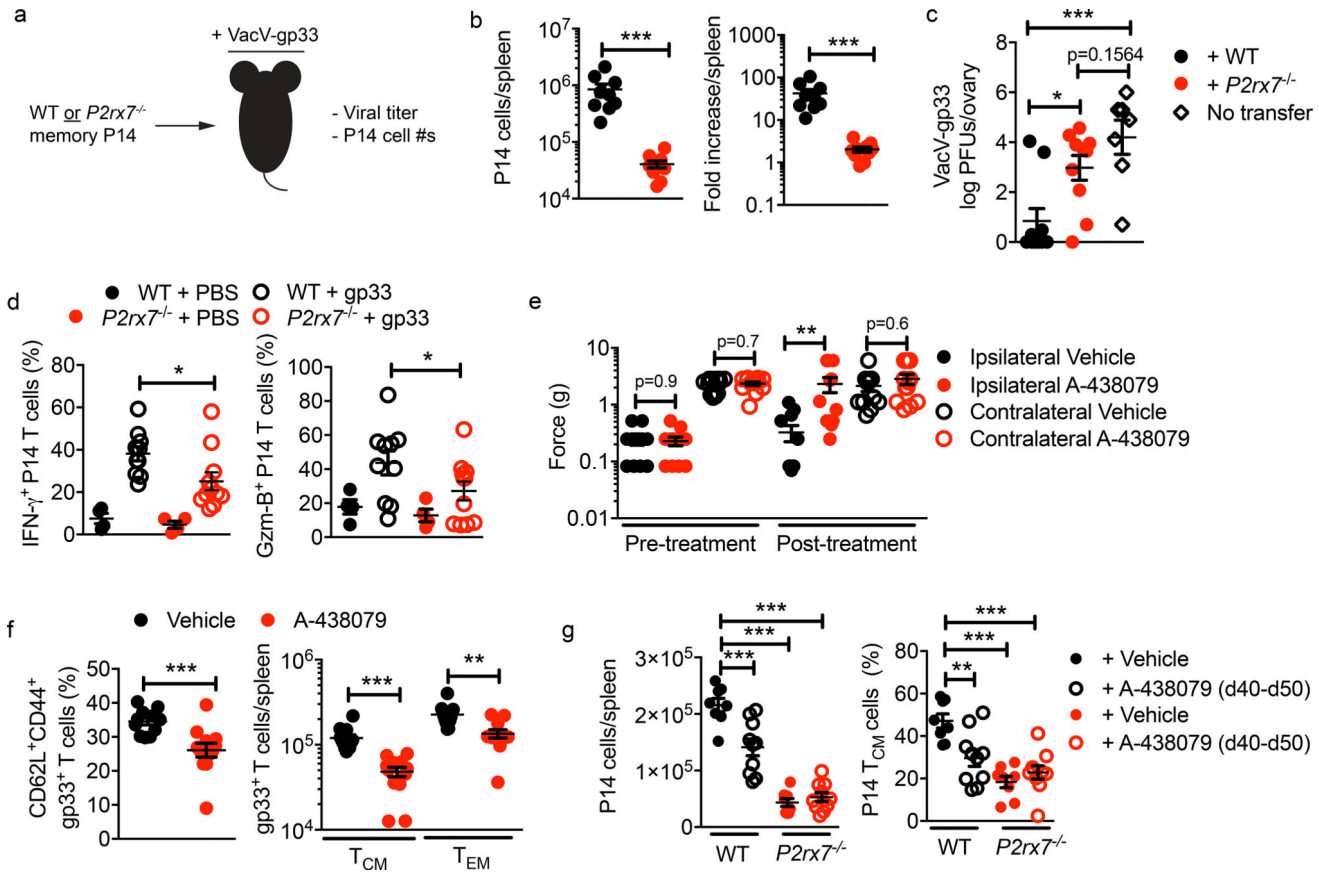

Fig. 4. P2RX7 promotes memory CD8$^+$ T cell function and P2RX7 blockade compromises CD8$^+$ T cell memory maintenance

(a–c) Memory WT or *P2rx7*$^{-/-}$ P14 were independently transferred into naïve recipient mice, which were then VacV-gp33-infected. **(b)** Splenic WT or *P2rx7*$^{-/-}$ P14 numbers (left) and fold increase (right) 7 days post-challenge. **(c)**, VacV-gp33 ovary viral titers 7 days post-challenge (log-transformed). **(d)**, WT and *P2rx7*$^{-/-}$ P14 cells were independently transferred and recipient mice primed with LCMV. After >30d, a transcervical challenge with gp33 or PBS was conducted and female reproductive tract (FRT) P14 12h later for IFN-γ production and Gzm-B expression. **(e–f)** B6 mice subjected to spare nerve injury were subsequently LCMV infected with/without A-438079 treatment. **(e)** mice were tested for pain sensitivity and **(f)** subsequent development of LCMV-specific ("gp33$^+$") splenic memory subsets. **(g)** mice were co-transferred and primed as in Fig. 1 and A-438079-treated 40–50 dpi. P14 numbers/spleen (left) and T_{CM} percentages (right) are shown. **(a–e)** Three independent experiments, n=9–10 (**a–b**), 7–10 (**c**), 4–11 (**d**) total. **(e–g)** Two independent experiments, n=12 (**e–f**), 8–10 (**h**) total. **(b–c,d–g)** mean ± SEM; **(b,e)**, Two-tailed Student's t-test; **(e–f)**, Two-tailed Mann-Whitney t-test; **(c,g)** One-way ANOVA + Tukey's post-test; *P≤0.05, **P≤0.01, ***P≤0.001.